Title: IL-17A-mediated alterations in gut microbiota composition, particularly changes in Prevotella abundance, impact Treg function in CNS Autoimmunity

Authors: Shailesh K. Shahi[1], Sudeep Ghimire[1], Samantha N. Jensen[1,2,†], Peter Lehman[1], Allison G Rux[1], Ti-Ara Turner[2], Nicholas Borcherding[3], Katherine N. Gibson-Corley[4], Sukirth M. Ganesan[5], Nitin J. Karandikar[1,2,], and Ashutosh K. Mangalam[1,2,6]*

Affiliations:

[1]Department of Pathology, University of Iowa, Iowa City, USA

[2]Graduate Program in Immunology, University of Iowa, Iowa City, USA

[3]Department of Pathology and Immunology, Washington University School of Medicine, Saint Louis, MO,

[4]Department of Pathology, Microbiology & Immunology; Vanderbilt University Medical Center, Nashville, TN

[5]Department of Periodontics College of Dentistry, University of Iowa, Iowa City, USA

[6]Iowa City VA Health Care System, Iowa City, IA 52246, USA

† Present address- Department of Microbiology and Immunology, Weill Cornell Medicine, Cornell University, New York, USA

***Corresponding Author**

Ashutosh K. Mangalam, Ph.D.
Department of Pathology,
University of Iowa Carver College of Medicine,
25 S. Grand Avenue, 1080A ML
Iowa City, IA 52242
Phone: 1-319-335-8558
Email. ashutosh-mangalam@uiowa.edu
ORCID 0000-0002-9926-2531

Abstract: A disrupted equilibrium among gut microbiota, IL-17A-producing CD4 T-cells (Th17), and regulatory CD4 T-cells (Treg) have been linked with the pathobiology of multiple sclerosis (MS). While gut microbiota can regulate both Treg and Th17 cells, the impact of IL-17A on this gut-immune connection remains unclear. Utilizing HLA-DR3 transgenic mouse model of MS, we show that IL-17A deficiency (HLA-DR3.IL17A$^{-/-}$) resulted in milder disease characterized by increased Tregs and expansion of Treg-promoting gut microbes, including *Prevotella*. Cohousing HLA-DR3 mice with HLA-DR3.IL17A$^{-/-}$ transferred the milder disease phenotype and associated microbiota changes to DR3 mice, highlighting the dominant role of gut microbiota in Treg induction and disease amelioration. DR3.IL17A$^{-/-}$ mice also showed a higher abundance of functional pathways linked with short-chain fatty acid synthesis and elevated IL-10 in dendritic cells. Enrichment of the Treg-promoting PPAR signaling pathway expression in the colon of HLA-DR3.IL17A$^{-/-}$ mice and following *Prevotella* administration in HLA-DR3 mice underscores the importance of gut microbiota in IL-17A-mediated immune regulation. Thus, our study uncovers a previously unappreciated role for IL-17A in shaping gut microbiota and immune regulation, with far-reaching implications for MS treatment.

Key Words: Immune regulation, IL-17A, gut microbiota, *Prevotella*, Tregs, Experimental Autoimmune Encephalomyelitis (EAE), multiple sclerosis

One-Sentence Summary: IL-17A modulates Treg and gut microbiota to control EAE.

Main text:

Multiple sclerosis (MS) is a chronic, inflammatory, neurodegenerative disease of the central nervous system (CNS), in which CD4 T helper (Th) cells of Th1 and/or Th17 phenotype have been shown to play an important role in pathobiology of the disease. IL-17A is a signature pro-inflammatory cytokine of the CD4 T helper 17 (Th17) subset that has emerged as being critical to the pathobiology of MS (1, 2). IL-17A plays a crucial role in resolving extracellular bacterial and fungal infections, by recruiting immune cells, specifically neutrophils, to the site of infection and inducing pro-inflammatory mediators from immune cells and fibroblasts, epithelial cells, and endothelial cells (3). However, an aberrant IL-17A response can lead to unresolved inflammation and tissue pathology, as observed in multiple autoimmune diseases, including MS (4, 5, 6, 7). Thus, although IL-17A is considered a major contributor to the pathogenesis of multiple autoimmune diseases, its precise role in the pathobiology of MS is still being explored. Th17 cells are regulated by $CD4^{+}CD25^{+}FoxP3^{+}$ regulatory T cells (Treg) and the balance between Treg/Th17 is shown to shift toward the Th17 phenotype in inflammatory diseases such as MS (8). Additionally, gut bacteria help maintain immune homeostasis by regulating the balance between $CD4^{+}CD25^{+}$FoxP3+ regulatory T cells (Tregs) and pro-inflammatory Th1/Th17 cells (9). The importance of gut microbiota in regulating the development of Treg and Th17 is highlighted by studies performed in germ-free mice where an absence of or reduced Treg and Th17 cells is evident. However, transplant of single bacterium such as segmented filamentous bacterium can restore Th17 (10) and a mixture of chloroform-resistant *Clostridium* (11) can induce/restore Treg population. These studies highlight the important role of gut microbiota in the regulation of the Th17 and Treg population and their role in the pathobiology of MS/EAE. However, whether IL-17A can regulate gut microbiota and/or Treg cells is unknown.

In addition to IL-17A, HLA class II genes, specifically HLA-DR2 and -DR3 alleles, are linked as the strongest genetic factors predisposing individuals to MS (12, 13, 14, 15, 16). We have previously utilized HLA-class II transgenic mice to validate the significance of HLA-class II molecules in the pathogenesis of MS (17, 18, 19, 20, 21). Additionally, we showed that loss of IFNγ was associated with increased IL-17A levels and severe disease in an HLA-class II transgenic mouse model of experimental autoimmune encephalomyelitis (EAE) (22). Collectively these data suggest that IL-17A might be responsible for severe disease in the absence of IFNγ, however it is unclear whether IL-17A is essential for disease induction or severity or both.

To elucidate the role of IL-17A in the pathogenesis of MS, we generated HLA-DR3 (DR3) class II transgenic mice lacking IL-17A (DR3.IL17A$^{-/-}$). Mice that express HLA-DR3 were chosen over other EAE models as our prior study suggested a role of IL-17A in disease severity in the absence of IFNγ (23). Unexpectedly, DR3.IL17A$^{-/-}$ transgenic mice were not resistant to EAE and developed EAE disease with similar disease incidence and onset. However, disease was milder compared to IL-17A-sufficient HLA-DR3 transgenic mice. In the absence of IL-17A, CD4^{+}CD25^{+}FoxP3^{+} Treg was expanded, in part due to enhanced growth of gut bacteria with the ability to induce Treg. Fecal transplant/cohousing studies confirmed the importance of gut bacteria in modulating IL-17A-mediated disease. IL-17A-sufficient mice that received fecal transplants and cohoused with IL-17A-deficient mice had lower EAE severity compared to DR3 transgenic mice. Mice lacking IL-17A (HLA-DR3.IL17A-/-) exhibited an enriched Treg-promoting PPAR signaling pathway, suggesting a link between gut bacteria and immune regulation. This same pathway showed increased expression after *Prevotella copri* administration in HLA-DR3 mice, further emphasizing the role of gut microbiota in influencing IL-17A-mediated immune responses. Finally, DR3.IL17A$^{-/-}$ transgenic mice showed enriched bacterial pathways for SCFA production and increased IL-10 from dendritic cells, suggesting an anti-inflammatory environment due to IL-17A deficiency. Thus, our study demonstrates that IL-17A regulates Treg levels by modulating the gut microbiota, which alters immune homeostasis and inflammation to promote EAE.

Materials and methods

Study design

The study utilized female HLA-DR3, HLA-DR3.IL17A$^{-/-}$ transgenic mice, DR3.IL17A$^{-/-}$IFNγ$^{-/-}$ transgenic mice and C57BL/6J mice to investigate the contributions of IL-17A to EAE. The disease was induced by immunizing mice with the PLP$_{91\text{-}110}$ peptide in HLA transgenic mice. C57BL/6 mice were immunized with MOG$_{35–55}$ peptide. The number of sample sizes are indicated in the Figure captions. The disease induction and scoring of the EAE was performed as described below and elsewhere (24). No data, including outliers, were excluded from the analysis. Experiments were performed at least twice with some exceptions as indicated in the Figure legends.

119 **Mouse procurement, disease induction, and scoring**

120 HLA-DR3 (DRA1*0101, DRB1*0301) transgenic mice on the B6/129 background have been
121 characterized previously (Das et al., 2000; Mangalam et al., 2009). These mice lack endogenous
122 murine major histocompatibility complex (MHC) class II genes ($AE^{-/-}$) and express alleles
123 DRA1*0101, DRB1*0301, as described previously (Das et al., 2000; Mangalam et al., 2009). The
124 HLA-DR3.IL17A$^{-/-}$ mice (referred to as DR3.IL17A$^{-/-}$) that were used in this study were generated
125 by crossing HLA-DR3 (referred to as DR3) and $AE^{-/-}$.IL17A$^{-/-}$ mice and validated using
126 genotyping. HLA-DR3 Transgenic mice were mated with IFNγ-deficient mice on B6 background
127 (Jackson Laboratory) to generate HLA-DRB1*0301.$AE^{-/-}$.IFN$\gamma^{-/-}$. DR3.IL17A$^{-/-}$IFN$\gamma^{-/-}$
128 transgenic mice were generated by crossing HLA-DR3.IL17$^{-/-}$ and HLA-DR3. IFN$\gamma^{-/-}$ mice and
129 validated using genotyping. C57BL/6 mice were also utilized in this study and were purchased
130 from the Jackson Laboratories (Bar Harbor, ME). Female DR3, DR3.IL17A$^{-/-}$, DR3.IL17A$^{-/-}$IFNγ^{-}
131 $^{/-}$, and C57BL/6 mice (8-10 weeks of age) were used in this study. Mice were bred and maintained
132 in the University of Iowa animal facility in accordance with NIH and institutional guidelines. All
133 experiments were approved by the Institutional Animal Care and Use Committee at the University
134 of Iowa.

135 To induce EAE in mice, DR3, DR3.IL17A$^{-/-}$, and DR3.IL17A$^{-/-}$IFN$\gamma^{-/-}$ transgenic mice (8 to 12
136 weeks old) were immunized subcutaneously in both flanks with 50 μg of $PLP_{91–110}$
137 (YTTGAVRQIFG DYKTTICGK) (GenScript, Piscataway NJ, USA) that was emulsified in CFA
138 containing 200 μg/mouse *Mycobacterium tuberculosis* H37Ra (Becton, Dickinson and Company,
139 Sparks, MD, USA). 80 ng of pertussis toxin (PTX) (Sigma Chemicals, St. Louis, MO; 100 ng) was
140 given intraperitoneal at day 0 and 2 post immunization. C57BL/6 mice were immunized
141 subcutaneously in both flanks with MOG_{35-55} CFA/PTX, as just described for immunization with
142 PLP (25). Mice were observed daily for disease symptoms and EAE was scored with the following
143 scoring system, as described previously (24): normal, 0; loss of tail tone, 1; hind limb weakness,
144 2; hind limb paralysis, 3; hind limb paralysis and forelimb paralysis or weakness, 4; and
145 morbidity/death, 5.

146

147 **Pathology**

148 Brains and spinal cords were collected from DR3, and DR3.IL17A$^{-/-}$ transgenic mice at day 30
149 post immunization. Histological analysis was performed to assess inflammation and
150 demyelination, as described previously (22, 26). Briefly, DR3 and DR3.IL17A$^{-/-}$ transgenic mice
151 were perfused with approximately 50 ml of 10% neutral buffered formalin via intracardiac
152 puncture. The calvaria and spinal columns were collected, and immersion fixed in 10 % neutral
153 buffered formalin (10% BFA) for 24-48 hours followed by decalcification in EDTA for
154 approximately 24 hours. Decalcified tissues were cut into 2 mm coronal blocks, embedded in
155 paraffin and routinely processed. The slides were cut at 4-5 mm thickness and stained with
156 hematoxylin and eosin. HE-stained slides including the brainstem, cortex, corpus callosum,
157 cerebellum, hippocampus, and striatum were examined and scored by a board-certified veterinary
158 pathologist as described previously (22, 26).

159

160 **Flow cytometry**

161 Peripheral blood mononuclear cells (PBMCs) were isolated from naïve DR3 and DR3.IL17A$^{-/-}$
162 transgenic mice using Histopaque-1077 (Millipore Sigma, USA) density centrifugation method as
163 per instructions from the manufacturer (Sigma-Aldrich, St. Louis, USA). Briefly, 200 µl of blood
164 was collected in an EDTA-containing Eppendorf tube by retroorbital bleeding. Blood was diluted
165 with 800 ml of phosphate-buffered saline (PBS; Gibco/Lubioscience) and added to 1 ml of
166 Histopaque-1077, and then centrifuged at 400 x g for 30 minutes at room temperature, without the
167 brake. Following centrifugation, the buffy coat was collected into 5 mL tubes and washed with
168 PBS (400 x g for 10 minutes at 4°C). The cells were washed with FACS buffer stained with
169 antibodies to detect surface expression of CD4 (GK1.5) and CD25 (PC61) (BD Biosciences,
170 Franklin Lakes, NJ), whereas intracellular expression of FoxP3^{+} was stained using an anti-
171 Mouse/Rat FoxP3 (FJK-16s) staining kit (eBiosciences, San Diego, CA). Intracellular staining for
172 IL17A was performed using the intracellular fixation permeabilization kit and anti-mouse IL17
173 (TC11-18H10.1) specific antibodies from eBioscience™. Cells were also stained with antibodies
174 to detect surface expression of CD45 (30-F11) and CD4 (clone GK1.5) to gate on the leukocyte
175 population.

176

177 **T cell proliferation and cytokine assay**

178 Mice were euthanized 10 days after immunization with $PLP_{91–110}$ and draining lymph nodes were
179 removed and challenged *in vitro* with $PLP_{91–110,}$ as described previously (27). The results are
180 presented as stimulation indices, which are counts per minute (cpm) of test sample/cpm of the
181 control). For cytokine analysis, supernatants were collected from culture 48 h after peptide
182 stimulation, and the concentration of cytokines (IL-17F) were measured by sandwich ELISA using
183 pairs of relevant anti-cytokine monoclonal antibodies (Pharmingen, San Diego, CA).

184

185 **Isolation of $CD4^+CD25^+$ Treg, $CD4^+CD25^-$ T effector, and Dendritic cells**

186 $CD4^+CD25^+$ T cells isolated from the spleens of DR3 and DR3.IL17A$^{-/-}$ transgenic mice using the
187 EasySep™ Mouse $CD4^+CD25^+$ regulatory T Cell Isolation Kit II (STEMCELL Technologies,
188 Vancouver, Canada) according to the manufacturer's protocols. $CD4^+CD25^-$ T effector cells were
189 isolated from the Treg-depleted fraction of splenocytes using Anti-Mouse CD4 Magnetic Particles
190 – DM (BD Biosciences, CA, USA). DCs were isolated from total splenocytes using CD11c
191 microbeads according to the manufacturer's protocols (BD Biosciences, CA, USA). The purity of
192 specific cell populations was analyzed by flow cytometry; all populations used were >90% pure.

193

194 ***In vivo* depletion of $CD4^+CD25^+$ Treg cells**

195 DR3 and DR3.IL17A$^{-/-}$ transgenic mice received two intraperitoneal injections (200 µg/injection)
196 of monoclonal anti-mouse CD25 (IL-2Ra) antibody (clone: PC-61.5.3; BioXcell) in 200 µl of PBS
197 per dose on days -5 and -3 before induction of EAE (28). Controls received two intraperitoneal
198 injections of 200 µl of PBS. $CD4^+CD25^+FoxP3^+$ T cell depletion was confirmed by flow
199 cytometric analysis of PBMCs on the day EAE was induced. For IL-17A depletion, DR3
200 transgenic mice were injected intraperitoneally with 100 ug/mouse anti-IL17A (Clone 17F3;
201 BioXcell), IgG1 (Clone MOPC-21; BioXcell) or PBS. IL-17A was blocked in C57BL/6 mice by
202 administering 100 ug/mouse anti-IL-17A, IgG1 or PBS by intraperitoneally injection every three
203 days following induction of EAE, starting at day 5 through day 32 (e.g., days -24, -21, -18, -15, -
204 12, -9, -6 and -3 pre EAE induction and post EAE induction (at day 5, 8, 11, 14, and 17). IL-17F

205 or GM-CSF cytokine inhibition was performed *in vivo* in DR3.IL17A$^{-/-}$ transgenic mice by
206 intraperitoneally injection of 100µg/mouse anti-IL-17F (clone; MM17F-8F5; BioXcell) or
207 100µg/mouse of anti-GM-CSF (clone; MP1-22E9; BioXcell) post induction of EAE on days 5,
208 10, and 14. Control DR3.IL17A$^{-/-}$ transgenic mice received 100µg/mouse IgG1 (Clone MOPC-21;
209 BioXcell).

210

211 **Treg suppression assay**

212 Spleens from 8-10-week-old DR3 and DR3.IL17A$^{-/-}$ transgenic mice were harvested for CD4^{+} T
213 cells by BD™ IMag Particles as per manufacturer instruction. T cell-depleted splenocytes were
214 used as antigen presenting cells after UV irradiation. CD4^{+}CD25^{+} T cells were isolated from
215 splenocytes of DR3 and DR3.IL17A$^{-/-}$ transgenic mice using EasySep™ Mouse CD4^{+}CD25^{+}
216 regulatory T cell isolation kit II (STEMCELL Technologies, Vancouver, Canada) according to the
217 manufacturer's protocols. Treg suppression assays were performed as described previously (29).

218

219 **Co-housing of DR3 and DR3.IL17A$^{-/-}$ transgenic mice**

220 For fecal transplantation, DR3.IL17A$^{-/-}$ transgenic mice were recipients of fecal transplants from
221 DR3 transgenic mice through oral gavage, and conversely, DR3 transgenic mice were recipients
222 of fecal transplants from DR3.IL17A$^{-/-}$ transgenic mice through oral gavage. Five days after oral
223 gavage, DR3 transgenic mice were cohoused with DR3.IL17A$^{-/-}$ transgenic mice. Fecal samples
224 were collected before and after co-housing for shotgun metagenomic sequencing.

225

226 **Microbiota DNA isolation, sequencing, and analysis**

227 Five female mice of each genotype, DR3 and DR3.IL17A$^{-/-}$, were assessed for the composition of
228 their gut microbiota before and after cohousing, resulting in a total of 20 fecal samples. DNA was
229 extracted using PowerSoil DNA Isolation Kit (Qiagen) following the manufacturer's protocol.
230 Each metagenomic DNA was quantified and sequenced using an Illumina MiSeq resulting in more
231 than 55 Gb of raw paired-end reads from 20 samples after shotgun metagenomic sequencing. The
232 raw paired-end metagenomes were quality trimmed using Trim Galore version 0.5.0 , followed by

233 host read filtering by mapping to the mouse genome (GRCm39) using Bowtie2 (30), with default
234 parameters resulting in 49.43 Gb of high-quality data. The quality trimmed and filtered forward
235 and reverse reads were taxonomically characterized using MetaPhlAN 3.0 and
236 mpa_v30_CHOCOPhlAN_201901 database with default parameter settings. The obtained relative
237 percentages of the microbial taxa were compared between the groups using the Kruskal-Wallis test
238 followed by Dunn's multiple t-tests in GraphPad Prism. The filtered and trimmed sequences were
239 further assembled using MegaHit (31). After assembly, Prokka was used to predict ORF based
240 protein coding genes and assign functions to the predicted genes (32). BBMap aligner was used to
241 produce quantifiable gene counts in the FPKM format (fragments per kilobase of gene per million)
242 (https://jgi.doe.gov/data-and- tools/bbtools/). InterProScan was utilized for assignment for KEGG
243 pathways and GO processes (https://www.ebi.ac.uk/interpro/search/sequence/). FPKM values of
244 every protein/gene assigned to each of the KEGG pathway or GO process were derived from
245 mapping the gene to the FPKM list of the genes identified in the previous step. Relative
246 abundances of genes and pathways were used for downstream statistical analysis. Statistical
247 significance between the groups were determined using non-parametric Wilcoxon signed rank test,
248 and data was visualized using GraphPad Prism.

249

250 **In vivo depletion of IL-17A in C57BL/6 mice**

251 C57BL/6 mice were placed in three groups that received antibody injections prior to EAE
252 induction (day -24, -21, -18, -15, -12, -9, -6, and -3): the first group of mice received intraperitoneal
253 injections (200 µg/injection) of monoclonal anti-mouse IL-17A (clone 17F3; BioXCell) in 200µl
254 PBS per dose; the second group of mice received 200 µg/injection of isotype control (mouse IgG1)
255 in 200µl PBS per dose; and the third group of mice received 200µl PBS to serve as vehicle control.
256 Similarly, three groups of C57BL/6 mice were treated with either monoclonal anti-mouse IL-17A
257 (200 µg/injection), isotype control mouse IgG1 (200 µg/injection), or PBS starting on day 5 post
258 EAE induction, and continuing every third day until day 32. Mice were observed daily for disease
259 symptoms and EAE was scored as per the scoring system described (33).

260

261 **Transcriptome sequencing and analysis**

262 Tissue sections from the colon of both DR3.IL17A$^{-/-}$ and DR3 mice before EAE induction were
263 collected, chopped into small pieces, stored in RNAlater (Millipore Sigma, MO, USA), and frozen
264 to -80^{0}C until further use. RNA was extracted using the RNeasy Kit (Qiagen) following the
265 manufacturer's instructions. The quality and quantity of the RNA was evaluated using a NanoDrop
266 and sequenced at Novogene Co. Ltd, CA. Sequences were quality controlled using default *fastqc*
267 and paired FASTQ files were aligned to the mm10 genome build with the kallisto pseudoaligner
268 (34) using 100 bootstraps. Estimated counts for transcripts were then aggregated into gene-level
269 quantifications based on gene symbol. An average of 14.79 ±1.3 million transcripts were obtained
270 for each sample. Further downstream processes were carried out in R 4.0.3 (35) using edgeR 3.32.1
271 (36) to identify differentially expressed genes, as described previously. Differentially expressed
272 genes were fed into ShinyGO (37) to identify changes to genes involved in KEGG database using
273 the mouse reference database.

274

275 **Quantification of PPAR Signaling Pathways Genes using qPCR**

276 Tissue sections from the colon of 8-weeks old DR3.IL17A$^{-/-}$ and DR3 mice were collected, and
277 RNA was extracted using the RNeasy Kit (Qiagen) following the manufacturer's instructions. The
278 quality and quantity of the RNA was evaluated using a NanoDrop. To determine the expression of
279 PPAR signaling pathway genes, namely *Adipoq*, *Plin1*, *Plin4*, and *Fabp4*, a two-step quantitative
280 reverse transcriptase-mediated real-time PCR (qPCR) was performed. Equal aliquots of total RNA
281 (2 µg) from colonic samples of DR3.IL17A$^{-/-}$ (n = 5) and DR3 mice (n = 5) were reverse
282 transcribed to cDNA using the High-Capacity iScript cDNA synthesis kit (Bio-Rad). qPCR
283 reactions were then carried out in triplicate using 50 ng of cDNA and the Applied Biosystems
284 Power SYBR Green PCR Master Mix (Applied Biosystems). Amplification data were collected
285 using an Applied Biosystems Prism 7900 sequence detector and analyzed with Sequence Detection
286 System software (Applied Biosystems). The qPCR primers for the genes were purchased from
287 Integrated DNA Technologies, Inc. The primer sequences used were as follows:
288 *Adipoq*: Fwd: AGATGGCACTCCTGGAGAGAAG, Rev: ACATAAGCGGCTTCTCCAGGCT
289 *Plin1*: Fwd: GAGAAGGTGGTAGAGTTCCTCC, Rev: GTGTGTCGAGAAAGAGTGTTGGC
290 *Plin4*: Fwd: GCACTAAGGACACGGTGACCAC, Rev: GACCACAGACTTGGTAGTGTCC
291 *Fabp4*: Fwd: TGAAATCACCGCAGACGACAGG, Rev: GCTTGTCACCATCTCGTTTTCTC

292 The data obtained from qPCR were normalized to the expression of the housekeeping gene
293 GAPDH.
294
295 To assess the effect of *Prevotella copri* (*P. copri* DSM 18205) treatment on the expression of
296 PPAR signaling pathway genes, DR3 mice were divided into two groups. One group of mice was
297 treated with *P. copri*, while the other group was treated with BHI media (control). The *P. copri*
298 group received 10^7 CFUs of live *P. copri* DSM 18205 via oral gavage every other day for a total
299 of seven doses. The control group received 200 µl of BHI media alone by oral gavage. Tissue
300 sections from the colon of *P. copri*-treated and BHI media-treated DR3 mice were collected, and
301 RNA extraction and qPCR analysis for the expression of PPAR signaling pathway genes (*Adipoq,*
302 *Plin1, Plin4,* and *Fabp4*), Treg, and IL10 genes were performed as described above.
303
304 **Data and materials availability:** All data needed to evaluate the conclusions in the manuscript
305 are present in the manuscript and/or the Supplementary Materials. Shotgun metagenomic
306 sequencing and RNA-seq data had been uploaded under bio-project PRJNA808406. No custom
307 codes were used for the data analysis.
308
309 **Results**
310 **IL-17A deficient HLA-class-DR3 transgenic mice develop milder EAE disease**
311 In the HLA class-II transgenic model of EAE, mice lacking IFNγ develop severe brain-specific
312 disease characterized by elevated levels of IL-17A (22). Thus, we hypothesized that in the absence
313 of IL-17A (DR3.IL17A$^{-/-}$), mice would be resistant to EAE. All transgenic mice developed
314 normally with no obvious signs of pathology, and analysis of splenocytes confirmed that these
315 mice lacked IL-17A-expressing CD4$^+$ T cells (Fig. S1).
316
317 Interestingly, both DR3 and DR3.IL17A$^{-/-}$ transgenic mice develop EAE disease with similar
318 disease onset and incidence (Fig. 1A, 1B). However, DR3.IL17A$^{-/-}$ transgenic mice developed
319 milder disease over time and had a significantly lower cumulative clinical EAE and peak EAE
320 score compared to DR3 mice (Fig. 1B, 1C, 1D). Histological analysis of the brain and spinal cord
321 tissues demonstrated milder inflammation and demyelination in DR3.IL17A$^{-/-}$ transgenic mice,
322 consistent with decreased inflammatory cell infiltration in CNS (Fig. 1E, 1F, 1G, 1H). Thus, our

323 data indicate that IL-17A is not required for the induction phase of the disease. However, the milder
324 disease that occurred in the absence of IL-17A over time suggests that it may play a role in disease
325 progression. To test this, we depleted IL-17A in DR3 transgenic mice by treating them with an
326 anti-IL-17A antibody before induction of EAE (Fig. 2). We treated mice with the anti-IL-17A
327 antibody on days -19, -14, -11, -8, and -4, before immunization with PLP_{91-110} for EAE induction
328 (Fig. 2A). Compared to the control group DR3 transgenic mice pre-treated with anti-IL-17A still
329 developed EAE however showed a milder disease course which was similar to EAE observed in
330 DR3.IL17A$^{-/-}$ transgenic mice (Fig. 2B, 2C). Thus, the development of milder disease in DR3 mice
331 in the absence of IL-17A (genetic deficiency and IL-17A neutralization) suggests IL-17A is
332 redundant for the induction phase of the disease but might be crucial for disease progression.
333
334 To determine if the effect of IL-17A on EAE disease was universal or limited to the HLA class II
335 transgenic mouse model, we assessed the effects of depleting IL-17A in wild-type C57BL/6J (B6)
336 mice which require immunization with MOG_{35-55} for EAE (38). B6 mice treated with anti-IL-17A
337 antibody after the onset of EAE (i.e., at days 5, 8, 11, 14, 17, 20, 23, 26, 29, and 32 post-disease
338 induction) showed significantly lower average clinical scores over time compared to mice treated
339 with PBS or IgG1a (Fig. S2A, S2B). Similar to DR3 transgenic mice, B6 mice that received pre-
340 treatment (i.e., at days -24,-21,-18,-15,-12,-9,-6, and -3) and post-treatment (days 5, 8, 11, 14, and
341 17) of anti-IL-17A antibody still developed EAE but exhibited lower disease severity (Fig. S2C,
342 S2D). These data indicated that the IL-17A is redundant for disease induction in both PLP-DR3-
343 EAE and MOG-B6-EAE models. Neutralization of IL-17A exacerbated EAE progression in both
344 HLA-DR3 and Wt B6 mice, suggesting a similar role of IL-17A in two models of MS disease.
345
346 Even though IL-17A is considered an important cytokine for the development of EAE (39), our
347 results suggest that IL-17A is crucial for disease progression rather than disease induction. It is
348 possible that IL-17F (shares 55% homology at the amino acid level with IL-17A) and other
349 inflammatory cytokines such as GM-CSF or IFNγ might compensate for IL-17A to induce disease.
350 We also found that IL-17A deficient mice have significantly higher levels of IL-17F compared to
351 IL-17A sufficient DR3 transgenic mice (Fig. S3). However, neutralizing IL-17F did not affect
352 disease incidence or severity (Fig. S4A, S4B, S4C). Next, we investigated whether GM-CSF was
353 compensating for EAE induction in IL-17A deficient mice, as GM-CSF is shown to be a

354 pathogenic cytokine in EAE (40). Although antigen specific CD4 T cells from DR3.IL17A$^{-/-}$
355 transgenic mice did not show increased levels of GM-CSF but neutralization of the GM-CSF in
356 DR3.IL17A$^{-/-}$ resulted in an increased average disease score at a later point of the disease (Fig.
357 S4A, S4B). However, the cumulative disease score was similar between isotype control and anti-
358 GM-CSF treated mice (Fig. S4C). Thus, our data suggested that niether GM-CSF nor IL-17F can
359 compensate for IL-17A in DR3.IL-17A$^{-/-}$ transgenic mice for disease induction. Further, to
360 determine the role of IFNγ in disease progression, we generated DR3 transgenic mice in which
361 both IFNγ and IL-17A were deleted (DR3.IL17A$^{-/-}$IFNγ$^{-/-}$). Interestingly, these mice still
362 developed diseases similar to those observed in DR3 transgenic mice (Fig. S5), suggesting that
363 neither IL-17A nor IFNγ is required for the development of EAE. Taken together, our data indicate
364 that neither IL-17A nor IL-17F nor GM-CSF nor IFNγ are required for the development of EAE
365 disease. Thus, our data point toward an inflammatory mediator besides IL-17A, IL-17F, IFNγ or
366 GM-CSF which is required for the induction of EAE disease.
367

368 **IL-17A deficiency enhances the proliferation of CD4^{+}CD25^{+}FOXP3^{+} Treg cells**

369 The milder course of EAE disease observed in IL-17A deficient mice suggested the possibility of
370 an immune-regulatory mechanism at play to dampen the chronic immune response. Studies have
371 shown that CD4^{+}CD25^{+}Foxp3^{+} regulatory T cells can regulate autoimmune inflammation in the
372 body and suppress IL-17A-secreting CD4+ Th17 cells (41, 42). Therefore, we analyzed the total
373 number of CD4^{+}CD25^{+}Foxp3^{+} regulatory T cells in the peripheral blood of DR3 and DR3.IL17A^{-}
374 $^{/-}$ mice. We observed that DR3.IL-17A$^{-/-}$ mice had a significantly higher percentage (Fig. 3A, 3B)
375 and number (Fig. 3C) of CD4^{+}CD25^{+}Foxp3^{+} regulatory T cells compared to DR3 mice. To
376 determine whether the increased Treg levels were responsible for milder disease phenotype in
377 DR3.IL17A$^{-/-}$ mice, we treated these mice with an anti-CD25 blocking antibody to neutralize the
378 Treg population as shown in Fig 3D and described previously (43). CD25 neutralization in
379 DR3.IL17A$^{-/-}$ mice resulted in severe disease phenotype similar to DR3 transgenic mice, indicating
380 that Treg were involved in establishing milder disease phenotype in DR3.IL17A$^{-/-}$ mice (Fig. 3E).
381 Notably, CD4^{+}CD25^{+} Treg that were isolated from the spleen of naïve DR3.IL17A$^{-/-}$ transgenic
382 mice had significantly higher suppressive ability against antigen specific CD4^{+}CD25^{-} effector cells
383 when compared to those of DR3 transgenic mice (Fig. 3F), further supporting the role of Treg in
384 determining clinical EAE outcomes in DR3.IL17A$^{-/-}$ transgenic mice. Collectively, our data

385 indicate that deficiency of IL-17A results in a higher frequency and number of $CD4^{+}CD25^{+}$ Treg
386 cells with a higher suppressive ability, which likely contributes to a milder disease phenotype in
387 DR3.IL-17A$^{-/-}$ transgenic mice.
388
389 **IL-17A deficiency modulates the composition of the gut microbiome**
390 The composition and function of the gut microbiota might impact the immune response. As the
391 gut microbiome is known to modulate the Treg, first, we hypothesized that the absence of IL-17A
392 modulated the composition of the gut microbiome, which then can induce the Treg population and
393 lead to a milder disease phenotype in DR3.IL17A$^{-/-}$ transgenic mice. Secondly, we hypothesize
394 that the microbiota enriched in IL-17A deficient mice, when transferred to IL-17A sufficient mice,
395 should alter the microbiota of DR3 transgenic mice to enhance Tregs in the gut.
396
397 To test our first hypothesis, we collected fecal samples from both DR3 and DR3.IL17A$^{-/-}$
398 transgenic mice before cohousing and performed shotgun metagenomic sequencing to characterize
399 the microbiome in these mice (Fig 4A). The microbial composition of DR3 transgenic mice
400 clustered distinctly from that of DR3.IL17A$^{-/-}$ mice (Fig. S6). Specifically, we observed a
401 significant increase in the average relative abundance of *Prevotella* sp. MGM1, *Parabacteroides*
402 *distasonis,* and *Bacteroides sartorii* in DR3.IL17A$^{-/-}$ mice (Fig. 4B, 4C, 4D, 4E). We did observe
403 that DR3.IL17A$^{-/-}$ mice had a significant reduction in the population of *B. vulgatus*,
404 *Lachnospiraceae* bacterium 10_1, *Lachnospiraceae* bacterium 28_4, *Lachnospiraceae* bacterium
405 COE1, and *Lachnospiraceae* bacterium A2 (Fig. 4F, 4G, 4H, 4I, 4J). A complete list of bacteria
406 showing trend but not reaching statistical significance have been provided in Figure S7.
407
408 For efficient microbiota transfer we first performed fecal transplantation through oral gavage
409 followed by cohousing as described previously (44, 45) . Microbiota analysis showed that the
410 microbial composition in DR3 transgenic mice shifted to become more similar to that in
411 DR3.IL17A$^{-/-}$ transgenic mice (Fig. 4B, Fig. S6). Specifically, *Prevotella* sp. MGM2 (Fig. 4K)
412 and *E. coli* (Fig. 4L) were present in DR3.IL17A$^{-/-}$ mice were significantly increased in DR3
413 transgenic mice after cohousing with DR3.IL17A$^{-/-}$ mice. *Prevotella* species were observed to be
414 significantly higher in DR3.IL17A$^{-/-}$ mice compared to DR3 transgenic mice prior to cohousing.
415 Specifically, *Prevotella* sp. MGM2 had significantly higher relative abundance in DR3 transgenic

416 mice after being cohoused with DR3.IL17A$^{-/-}$ mice. Also, *A. muciniphila*, and *H. typhlonius* were
417 absent in DR3 transgenic mice before they were cohoused but were increased but not significantly
418 after cohousing with DR3.IL17A$^{-/-}$ transgenic mice (Fig. 4B, Fig. S7). Similarly, the abundance of
419 *Prevotella* sp. MGM1, *P. distasonis* and *B. sartorii* were increased, although not to significant
420 levels, in DR3 transgenic mice after being cohoused with DR3.IL17A$^{-/-}$ transgenic mice (Fig. 4C,
421 4D, 4E). In contrast, *Lachnospiraceae* bacterial species (Fig. 4G, 4I and 4J) and *Muribaculaceae*
422 bacterium DSM 10370 (Fig. 4M) were significantly decreased in DR3 transgenic mice after being
423 cohoused with DR3.IL17A$^{-/-}$ transgenic mice. Thus, the cohousing of DR3 with DR3.IL17A$^{-/-}$
424 transgenic mice transformed microbiota by transferring *Prevotella* species in DR3 mice.
425
426 **Cohousing DR3 mice with DR3.IL17A$^{-/-}$ transgenic mice transfers a Treg-inducing**
427 **phenotype**
428 Next, we investigated whether that transferring the gut microbiome from DR3.IL17A$^{-/-}$ mice to
429 DR3 mice also affected Treg frequency and EAE severity. Therefore, we assessed the levels of
430 Treg in the peripheral blood for both IL-17A deficient and IL-17A sufficient mice after fecal
431 transplantation plus cohousing (Fig. 5A). We observed that CD4^{+}CD25^{+}FoxP3^{+} T cell populations
432 were significantly increased in DR3 transgenic mice after cohousing with DR3.IL17A$^{-/-}$ mice (Fig.
433 5B). In contrast, Treg populations were similar in DR3.IL17A$^{-/-}$ mice cohoused with DR3 mice
434 (Fig. 5C). These data suggest that microbes transferred from DR3.IL17A$^{-/-}$ transgenic mice to DR3
435 transgenic mice such as *Prevotella* species were crucial to enhance the Treg population.
436
437 Next, we examined whether cohousing also affected the outcome of the EAE disease phenotype.
438 DR3 and DR3.IL17A$^{-/-}$ transgenic mice were cohoused for four weeks and then housed separately
439 while EAE was induced, and the course of the disease was assessed. When housed separately, DR3
440 mice showed more severe disease than DR3.IL17A$^{-/-}$ mice as expected (Fig. 5D, 5E). In contrast,
441 DR3 mice cohoused with DR3.IL17A$^{-/-}$ mice showed milder disease compared to DR3 control
442 mice that were never cohoused (Fig 5D, 5E). However, the disease in DR3.IL-17$^{-/-}$ transgenic mice
443 were similar pre and post-cohousing with DR3 transgenic mice. Thus, our results confirmed that
444 the lack of IL-17A alters the composition of the gut microbiota to allow the expansion of bacteria
445 such as *Prevotella* species, leading to the expansion of the Treg population and ultimately, to
446 milder EAE disease phenotype.

447

448 **Short-chain fatty acid metabolic pathways are transferred from DR3.IL17A$^{-/-}$ transgenic**
449 **mice to DR3 transgenic mice after cohousing.**

450 Next, to identify the mechanism through which IL-17A-influenced gut microbiota can modulate
451 Treg, we compared bacterial metabolic pathways enriched in DR3.IL-17A$^{-/-}$ mice. We first
452 assessed short-chain fatty acids (SCFAs), as these have been previously reported to affect the
453 differentiation of T cells (46) and ameliorate EAE severity (47). The metabolic pathways
454 associated with pyruvate to propanoate (P108-PWY) and pyruvate fermentation to acetate and
455 lactate II (PWY-5100) trended higher, although not to significant levels, in DR3.IL17A$^{-/-}$
456 transgenic mice compared to DR3 transgenic mice before cohousing. P108-PWY was low in
457 abundance in both DR3 and DR3.IL17A$^{-/-}$ transgenic mice before cohousing but was significantly
458 higher in both strains after cohousing (Fig. S8A). Likewise, pyruvate fermentation to acetate and
459 lactate II was lower in DR3 transgenic mice but became significantly enriched after mice were
460 cohoused with DR3.IL17A$^{-/-}$ transgenic mice (Fig. S8B). The transfer of SCFA pathways from
461 DR3.IL17A$^{-/-}$ transgenic mice to DR3 transgenic mice, but not vice versa, indicates that the
462 DR3.IL17A$^{-/-}$ transgenic mice harbor microbes that are responsible for SCFAs production and
463 these microbes can be transferred to DR3 transgenic mice through co-housing. Thus, our data
464 suggests the potential role of microbiota mediated SCFAs production in inducing Treg to produce
465 milder disease in the absence of IL-17A.

466

467

468 **Loss of IL-17A enriches PPAR signaling genes in the colon of DR3 transgenic mice**

469 The majority of immune cells reside in the gut to protect its large surface area, and gut bacteria
470 play a vital role in generating these immune cells, especially Treg and Th17 cells. The importance
471 of gut microbiota in generation of Treg is highlighted by studies performed in germ-free/antibiotic
472 treated mice, which showed significantly reduced Treg population (48, 49). Therefore, to identify
473 whether the host genes involved in modulating the disease in IL-17A deficient mice, we performed
474 transcriptome analysis in the colonic tissues from naive DR3 and DR3.IL17A$^{-/-}$ mice (Fig. 6A).
475 We observed that the colonic tissues from mice of the different genotypes (e.g., DR3 and
476 DR3.IL17A$^{-/-}$) were distinctly separated (Fig. 6B). Upon differential analysis, we identified 123
477 genes that were differentially expressed in the colon between the two groups (Fig. 6C, Table S1).

478 Thirty-three out of 123 differentially expressed genes were upregulated in DR3.IL17$^{-/-}$ mice
479 relative to DR3 transgenic mice. PPAR signaling pathway was enriched upon KEGG database
480 search consisting of *Adipoq, Plin1, Plin4,* and *Fabp4* genes (Figure 6D, 6E), which was sufficient
481 to distinguish between the DR3 and DR3.IL17$^{-/-}$ mice. These genes were further validated using
482 qPCR where *Plin1, Plin4* and *Fabp4* and *Adipoq* were enriched with an average 5.07, 1.66, 3.12
483 folds in DR3.IL17A$^{-/-}$ transgenic mice compared to DR3 (Fig. 6F). PPAR signaling mainly
484 involves lipid synthesis, degradation, storage, transport, binding, oxidation, and cholesterol
485 metabolism. Interestingly, activation of PPAR pathways is shown to enhance Treg responses (50),
486 and inhibit the inflammatory response, producing significant anti-atherosclerosis (51) and Sjogren
487 Syndrome-like Dacryoadenitis (52) by modulating Th1/Th17 response. Especially, *Plin1* and
488 *Plin4* are involved with lipid storage, *Fabp4* with lipid binding, and *Adipoq* with lipid degradation
489 and previous study has demonstrated that lipid metabolism is closely associated with
490 improvements of mucosal barrier functions (53). Taken together, the upregulated genes in
491 DR3.IL17A$^{-/-}$ mice related to the PPAR signaling pathway suggest enrichment of Tregs exert an
492 anti-inflammatory effect in the colon. On the other hand, for the downregulated genes, pathways
493 belonging to alpha-linolenic acid and linoleic acid metabolism were enriched (Fig. S9A), and three
494 genes related to these pathways were sufficient to distinguish DR3 from DR3.IL17A$^{-/-}$ transgenic
495 mice (Fig. S9B).
496
497 Our microbiome and transcriptome data both indicated that there is enhanced Treg response in the
498 gut of DR3.IL17A$^{-/-}$ transgenic mice through transfer of *Prevotella* species. We have previously
499 shown that *Prevotella* species such as *P. histicola* increased the frequency and number of
500 CD4+FoxP3+ regulatory T cells in gut (54). Thus, we hypothesize that *Prevotella* species will
501 induce an anti-inflammatory effect in the colon by enhancing genes related to the PPAR signaling
502 pathway and finally affecting the Treg population. Hence, DR3 mice were either gavaged with *P.*
503 *copri* DSM 18205 (10^7CFU) or media control every alternate day for two weeks. Upon quantifying
504 the genes with qPCR, we observed that *Adipoq, Plin1* and *Fabp4* and *Plin4* genes were 8.26, 3.5,
505 1.2 and 2.67 average folds enriched in *P. copri* gavaged mice (Fig. 6G) suggesting that *P. copri*
506 may have induced the PPAR signaling pathway. Interestingly, FoxP3 and IL-10 were 4.98 and
507 14.6 average folds enriched in *P. copri* administered mice compared to control (Fig. 6G),

508 suggesting that *P. copri* treatment exerts anti-inflammatory effects in the colon by enhancing Tregs
509 and IL-10.
510
511 **Dendritic cells from DR3.IL17A$^{-/-}$ transgenic mice produce higher levels of IL-10**
512 We observed the transfer of *Prevotella* species and enrichment of Tregs in DR3 after cohousing
513 with DR3.IL17A$^{-/-}$. Thus, we asked if the antigen-presenting cells, such as dendritic cells (DCs) in
514 DR3 and DR3.IL17A$^{-/-}$ are primed by the gut microbiota to become tolerogenic. Therefore, we
515 analyzed the production of the anti-inflammatory cytokine IL-10 from LPS stimulated DCs from
516 naïve DR3 and DR3.IL17A$^{-/-}$ mice. Interestingly, CD11c^{+} DCs from naïve DR3.IL17A$^{-/-}$ mice
517 produced significantly higher levels of IL-10 compared to DR3 mice after stimulation with LPS
518 (Fig. 6H). Thus, CD11c+ DCs from DR3.IL17A$^{-/-}$ mice displayed a tolerogenic phenotype, marked
519 by increased IL-10 production and trended reduced antigen presentation, potentially contributing
520 to the milder disease course observed in these mice.
521
522 **Discussion**
523 IL-17A has been shown to play an important role in the pathobiology of autoimmune diseases,
524 including MS (4, 55, 56); however, the precise mechanism remains poorly understood. Here, we
525 demonstrate the crucial role of IL-17A in regulating the progression of EAE, an animal model of
526 MS. Our data showing milder disease but similar disease incidence and severity in DR3.IL17A$^{-/-}$
527 mice indicate an important role of IL-17A in regulating disease severity through modulation of
528 Treg populations and Treg-promoting gut bacteria like *Prevotella* species. The importance of Treg-
529 promoting gut bacteria was further validated by gut microbiota transfer utilizing cohousing
530 experiments. Specifically, co-housing IL-17A-sufficient DR3 transgenic mice with IL-17A-
531 deficient DR3.IL17A$^{-/-}$ transgenic mice altered gut microbiota composition and functions,
532 enrichment in the Treg subset, and a milder disease phenotype similar to that observed in
533 DR3.IL17A$^{-/-}$ transgenic mice. Furthermore, an analysis of host gene expression in the colon of
534 DR3.IL17A$^{-/-}$ transgenic mice compared to DR3 transgenic mice uncovered a crosstalk between
535 *Prevotella* species, the PPAR pathway, and Tregs in the gut. Thus, our results demonstrate an
536 intricate interplay between the host and gut microbes in relation to IL-17A, which ultimately
537 impacts the pathogenicity of central nervous system inflammatory diseases, such as MS.
538

539 The development of milder disease in DR3.IL17A$^{-/-}$ transgenic mice suggest induction of
540 regulatory pathways in the absence of IL-17A. In support of this, we observed an increased
541 CD4^{+}CD25^{+}FoxP3^{+} Treg population in DR3.IL17A$^{-/-}$ transgenic mice. Further, the disease was
542 restored after Treg depletion using an anti-CD25 (PC61) antibody, confirming an important role
543 for CD4^{+}CD25^{+} Treg subset in disease regulation. Interestingly, similar observations have also
544 been reported in GM-CSF deficient mice, which are resistant to EAE development, but treatment
545 with anti-CD25 antibody (PC61) resulted in the development of severe disease (57). Thus, these
546 data suggest that pathogenic cytokines such as IL-17A and GM-CSF might influence EAE disease
547 progression by downregulating regulatory cells such as CD4^{+}CD25^{+} Treg cells. Development of
548 disease in mice lacking IL-17A or receiving CD4^{+} T cells from *Csf2*-/- (mice lacking GM-CSF)
549 (57) supports our data that neither IL-17A nor GM-CSF are essential for disease development in
550 the EAE model.
551 Interestingly, we observed that IL-17A significantly affects disease progression without affecting
552 the onset of disease. This is consistent with other studies such as Haak et al., who showed that
553 either loss of IL-17A or overexpression of IL-17A in CNS has a major impact on disease
554 development (58). It is possible that other Th17 cytokines (IL-17F and GM-CSF) or even Th1
555 cytokine (IFNγ) can compensate for IL-17A loss for disease development. However, in our study,
556 mice that were treated with blocking antibodies against IL-17F or GM-CSF still developed the
557 disease. IL-17F is a member of the IL-17 family of cytokines, and several studies have investigated
558 its role in EAE. However, the majority of studies have concluded that IL-17F is either redundant
559 or does not play a role in EAE model (58, 59). IL-17F deficient mice treated with anti-IL-17A
560 blocking antibodies were susceptible to EAE (58). The role of GM-CSF in EAE and MS is still a
561 matter of debate, with some studies suggesting it is essential for EAE disease as GM-CSF deficient
562 mice are resistant to EAE development (60) whereas others have shown that GM-CSF is not
563 essential for EAE development (40, 61). Interestingly, Duncker et al., observed that although GM-
564 CSF is required for disease progression, it was dispensable for disease induction phase (40).
565 Development of severe disease in DR3 mice lacking both IL-17A and IFNγ ruled out the role of
566 IFNγ in disease induction in the absence of IL-17A. Thus, our data suggest that IL-17A, together
567 with IL-17F, GM-CSF, or IFNγ, is dispensable for the disease induction phase as DR3.IL-17A$^{-/-}$
568 transgenic mice still develop the disease, although in a milder course. Future studies will be
569 necessary to determine the mechanisms driving disease in the absence of IL-17A.

570

571 MS is driven by both host and environmental factors including gut microbiota, thus, both gut
572 microbiota and host genes can contribute to increased Treg population in DR3.IL17A$^{-/-}$ transgenic
573 mice. In recent years, gut microbiota has gained prominence as a significant contributor to the
574 induction and regulation of both Treg and Th17 cell subsets (49). Yet, our understanding of how
575 IL-17A affects the gut microbiome remains limited, and there have been suggestions that IL-17A/F
576 may function as modulators of intestinal microbiome and homeostasis (55). Indeed, in IL-17A
577 deficient DR3 transgenic mice, we observed an increase in abundance of gut bacteria such as
578 *Prevotella* species, *Parabacteroides distasonis,* and *Bacteroides species,* which are recognized for
579 their capacity to promote Treg population (33, 54, 62, 63). Specifically, *Prevotella* sps. MGM2
580 successfully transferred to the IL-17A sufficient mice from IL-17A deficient mice in high
581 numbers. Simultaneously, after cohousing IL-17A-deficient mice with IL-17A-sufficient mice,
582 none of the microbial species' abundances displayed significant alterations in IL-17A deficient
583 mice. After fecal transplantation or cohousing, the gut bacteria in DR3 mice became more similar
584 to that of DR3.IL17A$^{-/-}$ mice. This suggests that the gut microbiota of DR3.IL17A$^{-/-}$ mice is more
585 resistant to change, unlike the gut bacteria in DR3 mice. Ecologically, the degree of resistance of
586 the microbiota against incoming microbial species is crucial in determining health and disease
587 (64). The reduced stability and loss of resistance in the gut microbiota of DR3 transgenic mice was
588 reflected in increased disease severity, which was reduced upon cohousing with DR3.IL17A$^{-/-}$
589 transgenic mice. This suggests that the gut microbiota in DR3 transgenic mice underwent
590 reconfiguration to restore protective functions such as SCFAs production. SCFAs pathways
591 producing acetate, propionate, and lactate were present in DR3.IL17A$^{-/-}$ transgenic mice but not in
592 DR3 transgenic mice. SCFAs produced by gut bacteria are involved in enrichment/proliferation of
593 IL-10 producing Tregs and are crucial for maintaining gut homeostasis (65). In fact, the induction
594 of Treg in IL-17A deficient mice was concurrent with the increased production of IL-10 from
595 splenic DCs from DR3.IL17A$^{-/-}$ transgenic mice. It suggests that the tolerogenic DCs are induced
596 in the absence of IL-17A, and DC-derived IL-10 is essential to ameliorate EAE severity (66). The
597 reduced trends of antigen presentation capacity of DCs from DR3.IL17A$^{-/-}$ transgenic mice further
598 support the role of tolerogenic DCs in mice lacking IL-17A. Even, SCFAs such as propionate and
599 butyrate have been demonstrated as potent inducers of tolerogenic DCs (67). Thus, SCFAs
600 produced by the gut microbiota like *Prevotella* species in DR3.IL17A-/- transgenic mice can

601 induce tolerogenic DCs in IL-17A deficient mice. However, details of how the gut microbiota
602 affects DC proliferation and IL-10 production need to be investigated further.
603
604 On the host side, IL-17A-deficient mice, characterized by an increased Treg population and altered
605 gut microbiota composition, exhibited increased expression of PPAR signaling genes in our
606 transcriptome analysis. Genes belonging to PPAR signaling categories are indicated as important
607 mediators of anti-inflammatory responses (53, 68). Although a prior study involving both IL-17A
608 and IL-17F found no impact on Treg population (55), our findings reveal markedly elevated levels
609 of $CD4^{+}CD25^{+}FoxP3^{+}$ T cell populations in the DR3.IL17A$^{-/-}$ transgenic mice compared to DR3
610 transgenic mice suggesting a likely role of gut microbiome mediated Treg stimulation and anti-
611 inflammatory effect in the colon. *Prevotella* species were enriched in DR3.IL17A$^{-/-}$ transgenic
612 mice were later transferred through cohousing to DR3 transgenic mice, amplified Tregs in DR3
613 transgenic mice; we investigated if *Prevotella* species can, in fact, induce PPAR genes and Tregs.
614 We observed that *P. copri* DSM 18205 treatment to DR3 transgenic mice enriched colonic PPAR
615 pathways genes. Interestingly, along with enrichment of PPAR associated genes, *P. copri*
616 treatment to DR3 mice enriched FoxP3 and IL-10 gene expression in the colonic tissue. These
617 findings suggesting that *P. copri* treatment exerts anti-inflammatory effects in the colon by
618 enhancing the PPAR signaling pathway linked to Tregs and IL-10 induction. We have also
619 previously shown that introducing *Prevotella* species can alleviate EAE severity through changes
620 in the gut microbiota that ultimately promote Treg development (33, 54). Taken together, our study
621 demonstrates gut microbiota-dependent internal mechanisms to maintain intestinal homeostasis
622 and Treg function, and perturbation of the same can promote inflammation and CNS
623 autoimmunity. Suppression of disease in IL-17A sufficient mice on cohousing with IL-17A
624 deficient mice strongly suggests that Treg-promoting gut microbiota is dominant over disease-
625 promoting bacteria and thus has strong clinical translation potential. However, the microbial
626 community network and the interplay between the microbes in the community to exacerbate or
627 protect from EAE warrants deeper exploration.
628
629 In summary, our study highlights an important pathway through which IL-17A regulates
630 inflammation, specifically by modulating the gut microbiota to suppress Treg expansion. Our
631 study illuminates a novel mechanism by which immune mediators such as cytokines impact the

632 gut microbiota to alter immune cell function and, ultimately, disease outcomes. Our results have
633 strong clinical relevance as modulation of the gut microbiota are being considered as potential
634 therapeutics to treat diseases ranging from inflammatory to neurological diseases. As MS is an
635 inflammatory disease characterized by gut dysbiosis, combination therapies targeted to reduce
636 inflammation as well as correct gut dysbiosis might result in better therapeutic outcome than either
637 one alone. Although IL-17A had been linked with the pathobiology of MS, two anti-IL-17A
638 clinical trials in MS (NCT01874340 and NCT01433250) were terminated early. In that regard,
639 while anti-IL-17A therapy alone was not as effective as current MS drugs, a combination of anti-
640 IL-17A and microbiota modulation might provide better therapeutic efficacy. Additionally, Treg
641 induction is also being tried as a potential treatment option in MS (69). Our cohousing experiment
642 showing the ability of gut microbiota to colonize, induce Tregs, and suppress disease in susceptible
643 mice suggests that gut microbiota-based induction of host immunity might have an added
644 advantage as it will not only induce Tregs but can correct gut dysbiosis, too. Future studies testing
645 gut commensal with Treg-inducing capabilities in combination with anti-IL-17A are warranted to
646 test whether a combination of anti-inflammatory plus gut commensal modulation might provide
647 added benefits.
648

649

650 **References**

651 1. Korn T, Bettelli E, Oukka M, Kuchroo VK. IL-17 and Th17 Cells. Annu Rev Immunol. 2009;27:485-
652 517.
653 2. Milovanovic J, Arsenijevic A, Stojanovic B, Kanjevac T, Arsenijevic D, Radosavljevic G, et al.
654 Interleukin-17 in Chronic Inflammatory Neurological Diseases. Front Immunol. 2020;11:947.
655 3. Curtis MM, Way SS. Interleukin-17 in host defence against bacterial, mycobacterial and fungal
656 pathogens. Immunology. 2009;126(2):177-85.
657 4. Chong WP, Mattapallil MJ, Raychaudhuri K, Bing SJ, Wu S, Zhong Y, et al. The Cytokine IL-17A
658 Limits Th17 Pathogenicity via a Negative Feedback Loop Driven by Autocrine Induction of IL-24. Immunity.
659 2020;53(2):384-97 e5.
660 5. Biswas PS. IL-17 in Renal Immunity and Autoimmunity. J Immunol. 2018;201(11):3153-9.
661 6. Iwakura Y, Nakae S, Saijo S, Ishigame H. The roles of IL-17A in inflammatory immune responses
662 and host defense against pathogens. Immunol Rev. 2008;226:57-79.
663 7. McGeachy MJ, Cua DJ, Gaffen SL. The IL-17 Family of Cytokines in Health and Disease. Immunity.
664 2019;50(4):892-906.
665 8. Segal BM. Stage-specific immune dysregulation in multiple sclerosis. J Interferon Cytokine Res.
666 2014;34(8):633-40.
667 9. Weaver CT, Hatton RD. Interplay between the TH17 and TReg cell lineages: a (co-)evolutionary
668 perspective. Nat Rev Immunol. 2009;9(12):883-9.

669 10. Yang Y, Torchinsky MB, Gobert M, Xiong H, Xu M, Linehan JL, et al. Focused specificity of intestinal
670 TH17 cells towards commensal bacterial antigens. Nature. 2014;510(7503):152-6.
671 11. Atarashi K, Tanoue T, Oshima K, Suda W, Nagano Y, Nishikawa H, et al. Treg induction by a
672 rationally selected mixture of Clostridia strains from the human microbiota. Nature. 2013;500(7461):232-
673 6.
674 12. Alvarado-de la Barrera C, Zuniga-Ramos J, Ruiz-Morales JA, Estanol B, Granados J, Llorente L. HLA
675 class II genotypes in Mexican Mestizos with familial and nonfamilial multiple sclerosis. Neurology.
676 2000;55(12):1897-900.
677 13. DeLuca GC, Ramagopalan SV, Herrera BM, Dyment DA, Lincoln MR, Montpetit A, et al. An
678 extremes of outcome strategy provides evidence that multiple sclerosis severity is determined by alleles
679 at the HLA-DRB1 locus. Proceedings of the National Academy of Sciences of the United States of America.
680 2007;104(52):20896-901.
681 14. Dyment DA, Herrera BM, Cader MZ, Willer CJ, Lincoln MR, Sadovnick AD, et al. Complex
682 interactions among MHC haplotypes in multiple sclerosis: susceptibility and resistance. Hum Mol Genet.
683 2005;14(14):2019-26.
684 15. Olerup O, Hillert J. HLA class II-associated genetic susceptibility in multiple sclerosis: a critical
685 evaluation. Tissue antigens. 1991;38(1):1-15.
686 16. Ramagopalan SV, Deluca GC, Morrison KM, Herrera BM, Dyment DA, Lincoln MR, et al. Analysis
687 of 45 candidate genes for disease modifying activity in multiple sclerosis. Journal of neurology.
688 2008;255(8):1215-9.
689 17. Kaushansky N, Ben-Nun A. DQB1*06:02-Associated Pathogenic Anti-Myelin Autoimmunity in
690 Multiple Sclerosis-Like Disease: Potential Function of DQB1*06:02 as a Disease-Predisposing Allele. Front
691 Oncol. 2014;4:280.
692 18. Klehmet J, Shive C, Guardia-Wolff R, Petersen I, Spack EG, Boehm BO, et al. T cell epitope
693 spreading to myelin oligodendrocyte glycoprotein in HLA-DR4 transgenic mice during experimental
694 autoimmune encephalomyelitis. Clin Immunol. 2004;111(1):53-60.
695 19. Luckey D, Bastakoty D, Mangalam AK. Role of HLA class II genes in susceptibility and resistance to
696 multiple sclerosis: studies using HLA transgenic mice. J Autoimmun. 2011;37(2):122-8.
697 20. Nalawade SA, Ji N, Raphael I, Pratt A, 3rd, Kraig E, Forsthuber TG. Aire is not essential for regulating
698 neuroinflammatory disease in mice transgenic for human autoimmune-diseases associated MHC class II
699 genes HLA-DR2b and HLA-DR4. Cell Immunol. 2018;331:38-48.
700 21. Quandt JA, Huh J, Baig M, Yao K, Ito N, Bryant M, et al. Myelin basic protein-specific TCR/HLA-
701 DRB5*01:01 transgenic mice support the etiologic role of DRB5*01:01 in multiple sclerosis. J Immunol.
702 2012;189(6):2897-908.
703 22. Mangalam AK, Luo N, Luckey D, Papke L, Hubbard A, Wussow A, et al. Absence of IFN-gamma
704 increases brain pathology in experimental autoimmune encephalomyelitis-susceptible DRB1*0301.DQ8
705 HLA transgenic mice through secretion of proinflammatory cytokine IL-17 and induction of pathogenic
706 monocytes/microglia into the central nervous system. J Immunol. 2014;193(10):4859-70.
707 23. Mangalam A, Luckey D, Basal E, Behrens M, Rodriguez M, David C. HLA-DQ6 (DQB1*0601)-
708 restricted T cells protect against experimental autoimmune encephalomyelitis in HLA-DR3.DQ6 double-
709 transgenic mice by generating anti-inflammatory IFN-gamma. J Immunol. 2008;180(11):7747-56.
710 24. Shahi SK, Freedman SN, Dahl RA, Karandikar NJ, Mangalam AK. Scoring disease in an animal model
711 of multiple sclerosis using a novel infrared-based automated activity-monitoring system. Sci Rep.
712 2019;9(1):19194.
713 25. Tyler AF, Mendoza JP, Firan M, Karandikar NJ. CD8(+) T Cells Are Required For Glatiramer Acetate
714 Therapy in Autoimmune Demyelinating Disease. PLoS One. 2013;8(6):e66772.

715 26. Mangalam A, Luckey D, Basal E, Jackson M, Smart M, Rodriguez M, et al. HLA-DQ8 (DQB1*0302)-
716 restricted Th17 cells exacerbate experimental autoimmune encephalomyelitis in HLA-DR3-transgenic
717 mice. J Immunol. 2009;182(8):5131-9.
718 27. Mangalam AK, Luckey D, Giri S, Smart M, Pease LR, Rodriguez M, et al. Two discreet subsets of
719 CD8 T cells modulate PLP(91-110) induced experimental autoimmune encephalomyelitis in HLA-DR3
720 transgenic mice. J Autoimmun. 2012;38(4):344-53.
721 28. Goschl L, Preglej T, Hamminger P, Bonelli M, Andersen L, Boucheron N, et al. A T cell-specific
722 deletion of HDAC1 protects against experimental autoimmune encephalomyelitis. J Autoimmun.
723 2018;86:51-61.
724 29. Thornton AM, Shevach EM. CD4+CD25+ immunoregulatory T cells suppress polyclonal T cell
725 activation in vitro by inhibiting interleukin 2 production. J Exp Med. 1998;188(2):287-96.
726 30. Langmead B, Salzberg SL. Fast gapped-read alignment with Bowtie 2. Nat Methods.
727 2012;9(4):357-9.
728 31. Li D, Liu CM, Luo R, Sadakane K, Lam TW. MEGAHIT: an ultra-fast single-node solution for large
729 and complex metagenomics assembly via succinct de Bruijn graph. Bioinformatics. 2015;31(10):1674-6.
730 32. Seemann T. Prokka: rapid prokaryotic genome annotation. Bioinformatics. 2014;30(14):2068-9.
731 33. Mangalam A, Shahi SK, Luckey D, Karau M, Marietta E, Luo N, et al. Human Gut-Derived
732 Commensal Bacteria Suppress CNS Inflammatory and Demyelinating Disease. Cell Rep. 2017;20(6):1269-
733 77.
734 34. Bray NL, Pimentel H, Melsted P, Pachter L. Near-optimal probabilistic RNA-seq quantification. Nat
735 Biotechnol. 2016;34(5):525-7.
736 35. R Core Team. R: A language and environment for statistical computing R Foundation for Statistical
737 Computing, Vienna, Austria. 2020.
738 36. Robinson MD, McCarthy DJ, Smyth GK. edgeR: a Bioconductor package for differential expression
739 analysis of digital gene expression data. Bioinformatics. 2010;26(1):139-40.
740 37. Ge SX, Jung D, Yao R. ShinyGO: a graphical gene-set enrichment tool for animals and plants.
741 Bioinformatics. 2020;36(8):2628-9.
742 38. Jensen SN, Cady NM, Shahi SK, Peterson SR, Gupta A, Gibson-Corley KN, et al. Isoflavone diet
743 ameliorates experimental autoimmune encephalomyelitis through modulation of gut bacteria depleted
744 in patients with multiple sclerosis. Sci Adv. 2021;7(28).
745 39. Komiyama Y, Nakae S, Matsuki T, Nambu A, Ishigame H, Kakuta S, et al. IL-17 plays an important
746 role in the development of experimental autoimmune encephalomyelitis. J Immunol. 2006;177(1):566-
747 73.
748 40. Duncker PC, Stoolman JS, Huber AK, Segal BM. GM-CSF Promotes Chronic Disability in
749 Experimental Autoimmune Encephalomyelitis by Altering the Composition of Central Nervous System-
750 Infiltrating Cells, but Is Dispensable for Disease Induction. J Immunol. 2018;200(3):966-73.
751 41. Li Z, Li D, Tsun A, Li B. FOXP3+ regulatory T cells and their functional regulation. Cell Mol Immunol.
752 2015;12(5):558-65.
753 42. Hori S, Nomura T, Sakaguchi S. Control of regulatory T cell development by the transcription factor
754 Foxp3. Science. 2003;299(5609):1057-61.
755 43. Christensen AD, Skov S, Kvist PH, Haase C. Depletion of regulatory T cells in a hapten-induced
756 inflammation model results in prolonged and increased inflammation driven by T cells. Clin Exp Immunol.
757 2015;179(3):485-99.
758 44. Montgomery TL, Kunstner A, Kennedy JJ, Fang Q, Asarian L, Culp-Hill R, et al. Interactions between
759 host genetics and gut microbiota determine susceptibility to CNS autoimmunity. Proceedings of the
760 National Academy of Sciences of the United States of America. 2020;117(44):27516-27.
761 45. Ridaura VK, Faith JJ, Rey FE, Cheng J, Duncan AE, Kau AL, et al. Gut microbiota from twins
762 discordant for obesity modulate metabolism in mice. Science. 2013;341(6150):1241214.

763 46. Haghikia A, Jorg S, Duscha A, Berg J, Manzel A, Waschbisch A, et al. Dietary Fatty Acids Directly
764 Impact Central Nervous System Autoimmunity via the Small Intestine. Immunity. 2015;43(4):817-29.
765 47. Mizuno M, Noto D, Kaga N, Chiba A, Miyake S. The dual role of short fatty acid chains in the
766 pathogenesis of autoimmune disease models. PLoS One. 2017;12(2):e0173032.
767 48. Atarashi K, Tanoue T, Shima T, Imaoka A, Kuwahara T, Momose Y, et al. Induction of colonic
768 regulatory T cells by indigenous Clostridium species. Science. 2011;331(6015):337-41.
769 49. Round JL, Mazmanian SK. Inducible Foxp3+ regulatory T-cell development by a commensal
770 bacterium of the intestinal microbiota. Proceedings of the National Academy of Sciences of the United
771 States of America. 2010;107(27):12204-9.
772 50. Miao Y, Zhang C, Yang L, Zeng X, Hu Y, Xue X, et al. The activation of PPARgamma enhances Treg
773 responses through up-regulating CD36/CPT1-mediated fatty acid oxidation and subsequent N-glycan
774 branching of TbetaRII/IL-2Ralpha. Cell Commun Signal. 2022;20(1):48.
775 51. Gao Z, Xu X, Li Y, Sun K, Yang M, Zhang Q, et al. Mechanistic Insight into PPARgamma and Tregs in
776 Atherosclerotic Immune Inflammation. Front Pharmacol. 2021;12:750078.
777 52. Guo X, Dang W, Li N, Wang Y, Sun D, Nian H, et al. PPAR-alpha Agonist Fenofibrate Ameliorates
778 Sjogren Syndrome-Like Dacryoadenitis by Modulating Th1/Th17 and Treg Cell Responses in NOD Mice.
779 Invest Ophthalmol Vis Sci. 2022;63(6):12.
780 53. Wei X, Yang Z, Rey FE, Ridaura VK, Davidson NO, Gordon JI, et al. Fatty acid synthase modulates
781 intestinal barrier function through palmitoylation of mucin 2. Cell Host Microbe. 2012;11(2):140-52.
782 54. Shahi SK, Freedman SN, Murra AC, Zarei K, Sompallae R, Gibson-Corley KN, et al. Prevotella
783 histicola, A Human Gut Commensal, Is as Potent as COPAXONE(R) in an Animal Model of Multiple Sclerosis.
784 Front Immunol. 2019;10:462.
785 55. Regen T, Isaac S, Amorim A, Nunez NG, Hauptmann J, Shanmugavadivu A, et al. IL-17 controls
786 central nervous system autoimmunity through the intestinal microbiome. Sci Immunol. 2021;6(56).
787 56. McGinley AM, Sutton CE, Edwards SC, Leane CM, DeCourcey J, Teijeiro A, et al. Interleukin-17A
788 Serves a Priming Role in Autoimmunity by Recruiting IL-1beta-Producing Myeloid Cells that Promote
789 Pathogenic T Cells. Immunity. 2020;52(2):342-56 e6.
790 57. Ghosh D, Curtis AD, 2nd, Wilkinson DS, Mannie MD. Depletion of CD4+ CD25+ regulatory T cells
791 confers susceptibility to experimental autoimmune encephalomyelitis (EAE) in GM-CSF-deficient Csf2-/-
792 mice. J Leukoc Biol. 2016;100(4):747-60.
793 58. Haak S, Croxford AL, Kreymborg K, Heppner FL, Pouly S, Becher B, et al. IL-17A and IL-17F do not
794 contribute vitally to autoimmune neuro-inflammation in mice. J Clin Invest. 2009;119(1):61-9.
795 59. Wanke F, Tang Y, Gronke K, Klebow S, Moos S, Hauptmann J, et al. Expression of IL-17F is
796 associated with non-pathogenic Th17 cells. J Mol Med (Berl). 2018;96(8):819-29.
797 60. McQualter JL, Darwiche R, Ewing C, Onuki M, Kay TW, Hamilton JA, et al. Granulocyte macrophage
798 colony-stimulating factor: a new putative therapeutic target in multiple sclerosis. J Exp Med.
799 2001;194(7):873-82.
800 61. Pierson ER, Goverman JM. GM-CSF is not essential for experimental autoimmune
801 encephalomyelitis but promotes brain-targeted disease. JCI Insight. 2017;2(7):e92362.
802 62. Cekanaviciute E, Yoo BB, Runia TF, Debelius JW, Singh S, Nelson CA, et al. Gut bacteria from
803 multiple sclerosis patients modulate human T cells and exacerbate symptoms in mouse models. Proc Natl
804 Acad Sci U S A. 2017;114(40):10713-8.
805 63. Nutsch KM, Hsieh CS. T cell tolerance and immunity to commensal bacteria. Curr Opin Immunol.
806 2012;24(4):385-91.
807 64. Lozupone CA, Stombaugh JI, Gordon JI, Jansson JK, Knight R. Diversity, stability and resilience of
808 the human gut microbiota. Nature. 2012;489(7415):220-30.
809 65. Sun M, Wu W, Chen L, Yang W, Huang X, Ma C, et al. Microbiota-derived short-chain fatty acids
810 promote Th1 cell IL-10 production to maintain intestinal homeostasis. Nat Commun. 2018;9(1):3555.

811 66. Kashi VP, Ortega SB, Karandikar NJ. Neuroantigen-specific autoregulatory CD8+ T cells inhibit
812 autoimmune demyelination through modulation of dendritic cell function. PLoS One. 2014;9(8):e105763.
813 67. Kaisar MMM, Pelgrom LR, van der Ham AJ, Yazdanbakhsh M, Everts B. Butyrate Conditions Human
814 Dendritic Cells to Prime Type 1 Regulatory T Cells via both Histone Deacetylase Inhibition and G Protein-
815 Coupled Receptor 109A Signaling. Front Immunol. 2017;8:1429.
816 68. Sohn JH, Lee YK, Han JS, Jeon YG, Kim JI, Choe SS, et al. Perilipin 1 (Plin1) deficiency promotes
817 inflammatory responses in lean adipose tissue through lipid dysregulation. J Biol Chem.
818 2018;293(36):13974-88.
819 69. Chwojnicki K, Iwaszkiewicz-Grzes D, Jankowska A, Zielinski M, Lowiec P, Gliwinski M, et al.
820 Administration of CD4(+)CD25(high)CD127(-)FoxP3(+) Regulatory T Cells for Relapsing-Remitting Multiple
821 Sclerosis: A Phase 1 Study. BioDrugs. 2021;35(1):47-60.

822

823 **Acknowledgements:** We thank the Waldschmidt, Legge, Jabbari, and Lieberman laboratories for
824 helpful discussion. We thank Jian Zhang and John Harty for reading the manuscript and providing
825 their valuable input. We also thank the Comparative Pathology Laboratory at the University of
826 Iowa, Department of Pathology, for their time and efforts.

827

828 **Funding:** We acknowledge funding from following sources-
829 National Institutes of Health/NIAID 1R01AI137075 (AKM)
830 Veteran Affairs Merit Award 1I01CX002212 (AKM)
831 Veteran Affairs Merit Award 1I01BX006112 (AKM)
832 University of Iowa Environmental Health Sciences Research Center, NIEHS/NIH P30 ES005605
833 (AKM)
834 Gift from P. Heppelmann and M. Wacek to (AKM)
835 Carver Trust Pilot Grant (AKM)
836 National Institute of Health training grant in Immunology T32AI007485 PI- G. Bishop/K Legge
837 (SNJ and TT)

838

839 **Author Contributions:**
840 Conceptualization: AKM, SKS, NJK
841 Formal analysis: SKS, SG, NB, KNGC, SMG
842 Methodology: AKM, SKS, NB, NJK
843 Investigation: AKM, SKS, SNJ, SG, AGR, TT, NB, PL, AGR, TT, KNGC
844 Visualization: AKM, SKS, SNJ, SG, TT, NB, KNGC, SMG
845 Funding acquisition: AKM

Project administration: AKM, SKS

Supervision: AKM, NJK

Writing – original draft: AKM, SKS, SG,

Writing – review & editing: AKM, SKS, SG, SMG, NJK

Competing interests: AKM is inventor of a technology claiming the use of *Prevotella histicola* for the treatment of autoimmune diseases. The patent for the technology is owned by Mayo Clinic, who has given exclusive license to Evelo Biosciences. AKM received royalties from Mayo Clinic (paid by Evelo Biosciences). However, no fund or product from the patent were used in the present study.

The remaining authors declare that the research was conducted in the absence of any commercial or financial relationships that could be construed as a potential conflict of interest.

860 **Figures:**

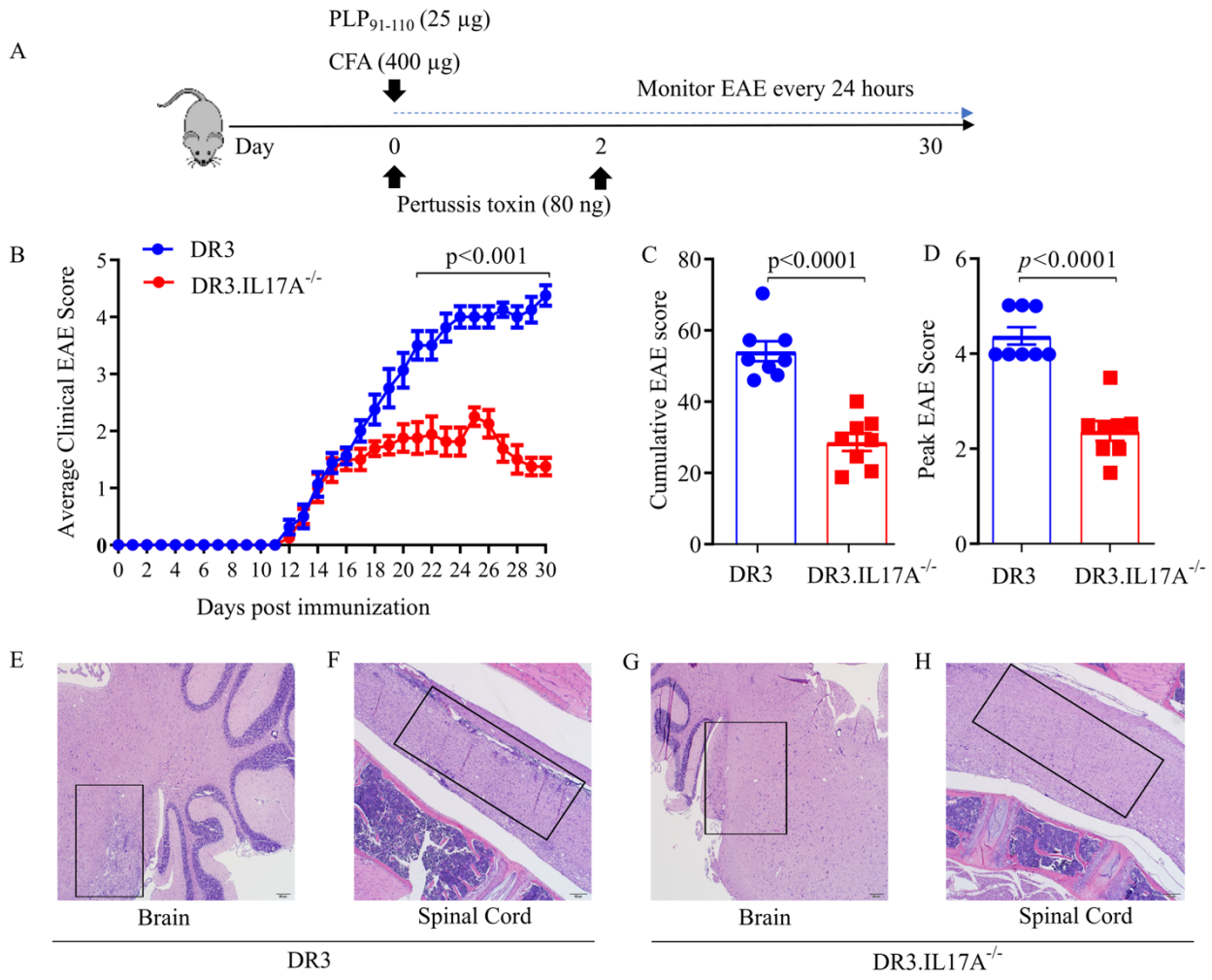

861

862 **Fig. 1: IL-17A deficiency ameliorates EAE in DR3 transgenic mice** (**A**) Schematic design of
863 disease course in DR3 mice. DR3 (n= 8) and DR3.IL17A$^{-/-}$ (n= 8) mice were immunized with
864 PLP$_{91-110}$ /CFA at day 0 and Pertussis toxin at days 0 and 2 to induce EAE. Mice were monitored
865 for EAE disease progression before euthanizing on day 30 post-immunization. (**B**) Clinical EAE
866 scores from mice in A, acquired over time. (**C**) Cumulative EAE scores from mice in A. (**D**) Peak
867 EAE score from mice in A. (**E-H**) Representative histological images of tissues from the CNS
868 from mice in A. Data are representative of 3 independent experiments with 4-5 mice per group.
869 Bullet points (B) or bars (C, D) represent the mean and error bars represent the standard error of
870 the mean for each experimental group. *p*-value was determined by multiple unpaired t-test (B),
871 and unpaired t-test with Welch correction (C, D).

872

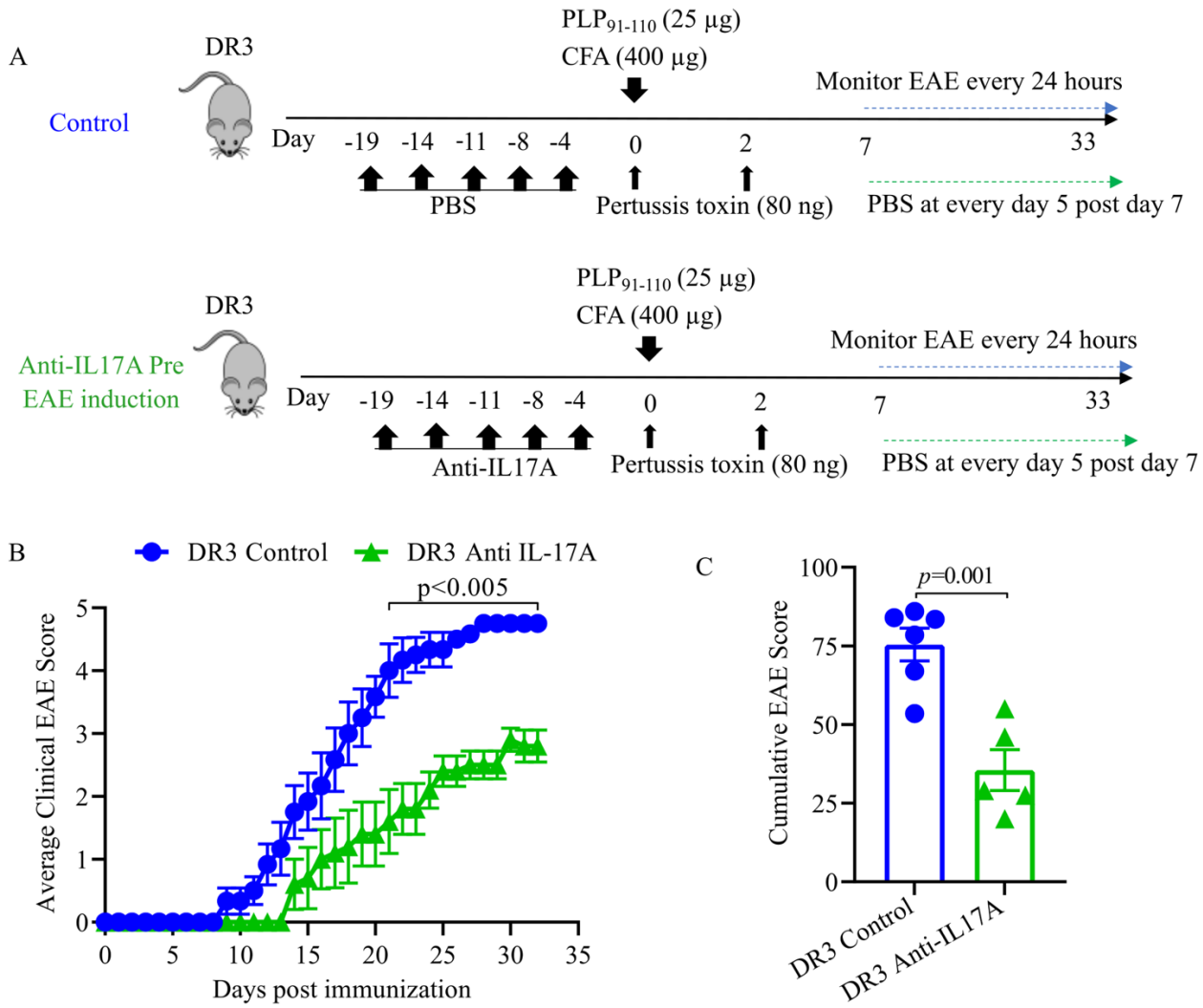

Fig. 2: Anti-IL-17A treatment reduces the severity of EAE in DR3 mice. (**A**) Schematic design of anti-IL-17A treatment in mice induced with EAE. 8-10-week-old DR3 mice were treated with an anti-IL-17A monoclonal antibody before EAE induction with PLP_{91-110}/CFA. (**B**) Average clinical EAE scores of mice treated as in A. Bullet points represent the mean and bars represent the standard error of the mean of each experimental group. (**C**) Average cumulative EAE scores of mice in A. Bars represent the mean and standard error of mean in each group. Data are from two independent experiments (n ≥4 mice per group). *p*-value determined by multiple unpaired t-test (B) and unpaired t-test with Welch correction (C).

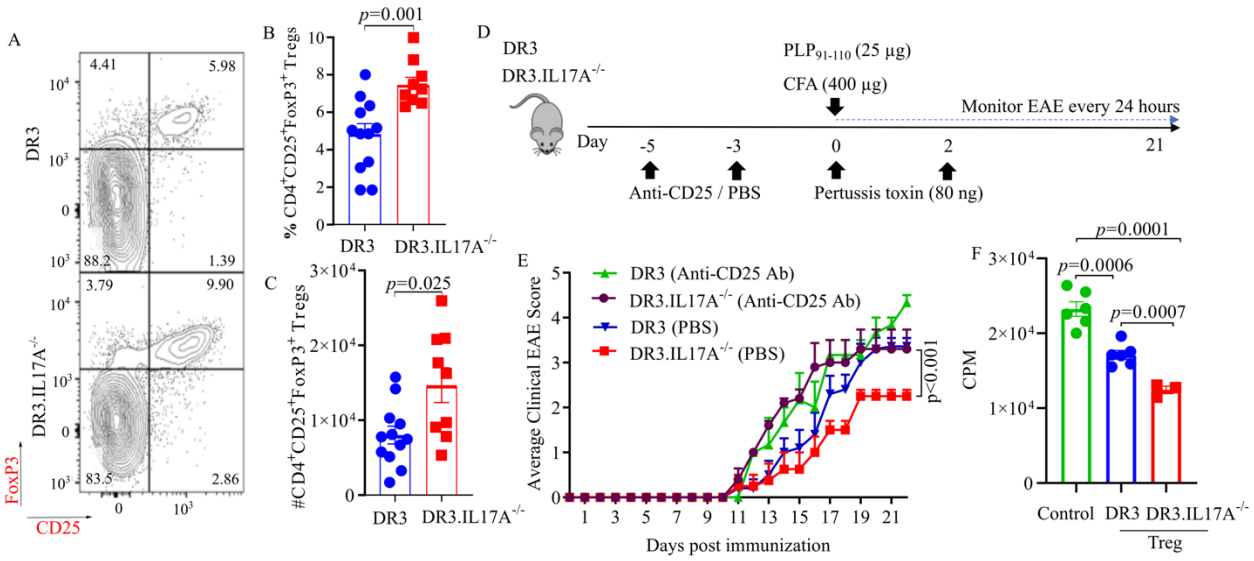

Fig. 3: IL-17A deficiency in DR3 transgenic mice results in expansion of CD4$^+$CD25$^+$FOXP3$^+$ Treg cells. (**A**) Representative flow cytometric plots of peripheral blood mononuclear cells (PBMCs) isolated from 8-10-week-old DR3 and DR3.IL17A$^{-/-}$ transgenic mice. Plots were gated on live lymphocytes and singlets. (B) Percentage and (C) total number of CD4$^+$CD25$^+$FoxP3$^+$ regulatory T cells from mice shown in A. (**D**) Schematic diagram of experimental workflow. DR3 and DR3.IL17A$^{-/-}$ transgenic mice were treated with anti-CD25 to neutralize Treg prior to immunization with PLP$_{91-110}$ /CFA to induce EAE. Arrowheads represent days in which mice received anti-CD25 treatment. (**E**) Average clinical EAE scores of DR3 and DR3.IL17A$^{-/-}$ mice that were treated with anti-CD25 or PBS prior to induction of EAE. (**F**) Counts per minute (CPM) of DR3 CD4 effector cells and antigen presenting cells cultured with CD4$^+$CD25$^+$ Treg from the spleen of naïve DR3 or DR3.IL17A$^{-/-}$ transgenic mice. The data represent two experiments performed at different time points. Bars represent the mean and standard error of the mean from two independent experiments. n =4-8 mice per group. *p*-value was determined by unpaired t-test with Welch correction (B, C, F) and two-way ANOVA for EAE clinical scores (E).

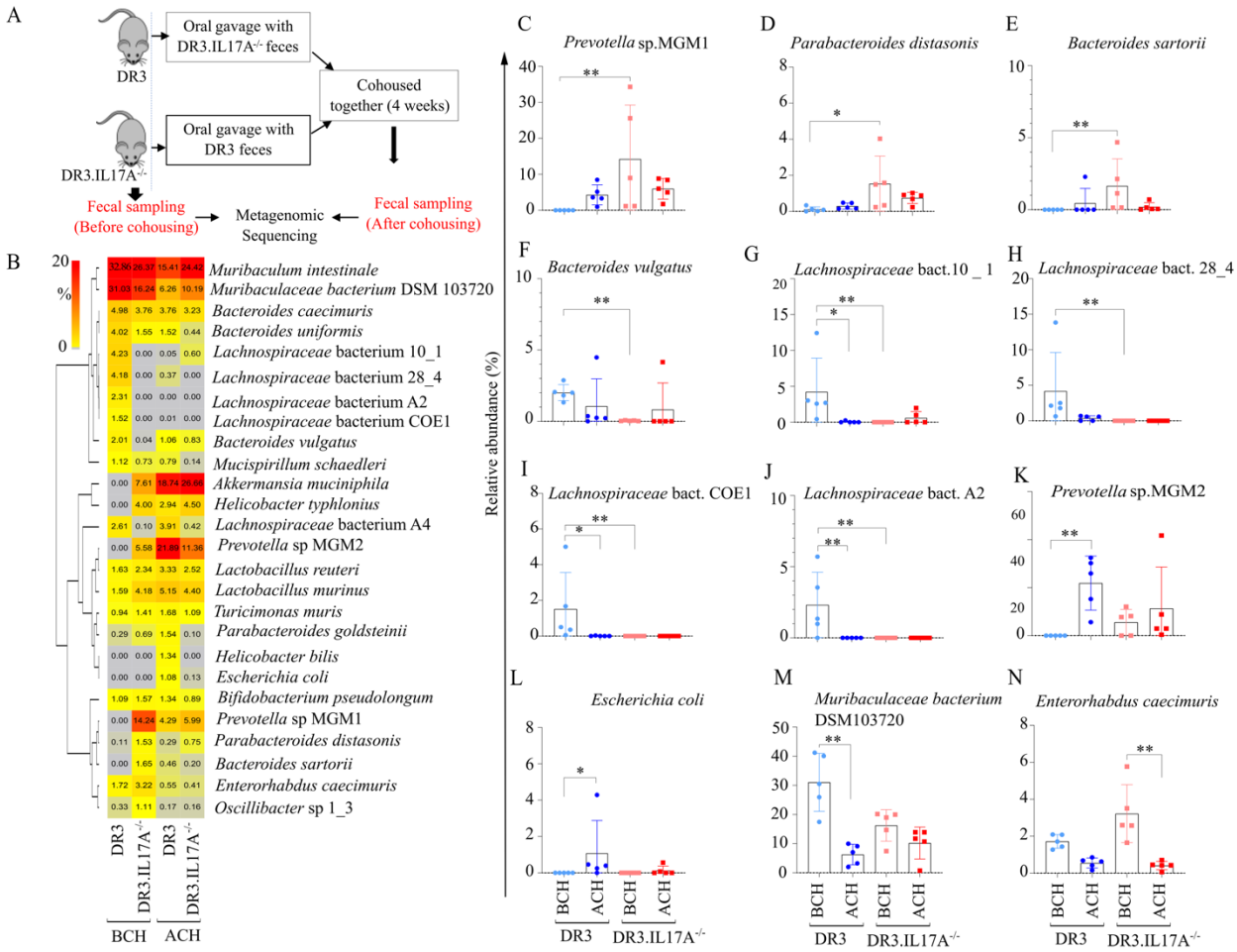

Fig. 4: Taxonomic characterization of the gut microbiome in DR3 and DR3.IL17A$^{-/-}$ mice. Fecal samples from DR3 and DR3.IL-17A$^{-/-}$ transgenic mice before cohousing (BCH), or after that one time fecal transferred (orally gavaged) and cohoused (ACH) were obtained and subjected to shotgun metagenomic sequencing. (**A**) Schematic diagram representing the experimental flow. (B) Heatmap depicting bacterial species with > 1% average relative abundance in at least one group (n=5). (**C-N**). Statistically significantly abundant bacterial taxa that were statistically different in abundance in at least one of the comparisons (e.g., DR3-BCH to DR3.IL17A$^{-/-}$-BCH, DR3-BCH to DR3-ACH, and DR3.IL17A$^{-/-}$-BCH to DR3.IL17A$^{-/-}$-ACH). Kruskal Wallis test followed by Dunn's *posthoc* analysis was performed to identify significant differences between groups. "*" and "**" represent significance at $p<0.05$ and $p<0.01$ respectively.

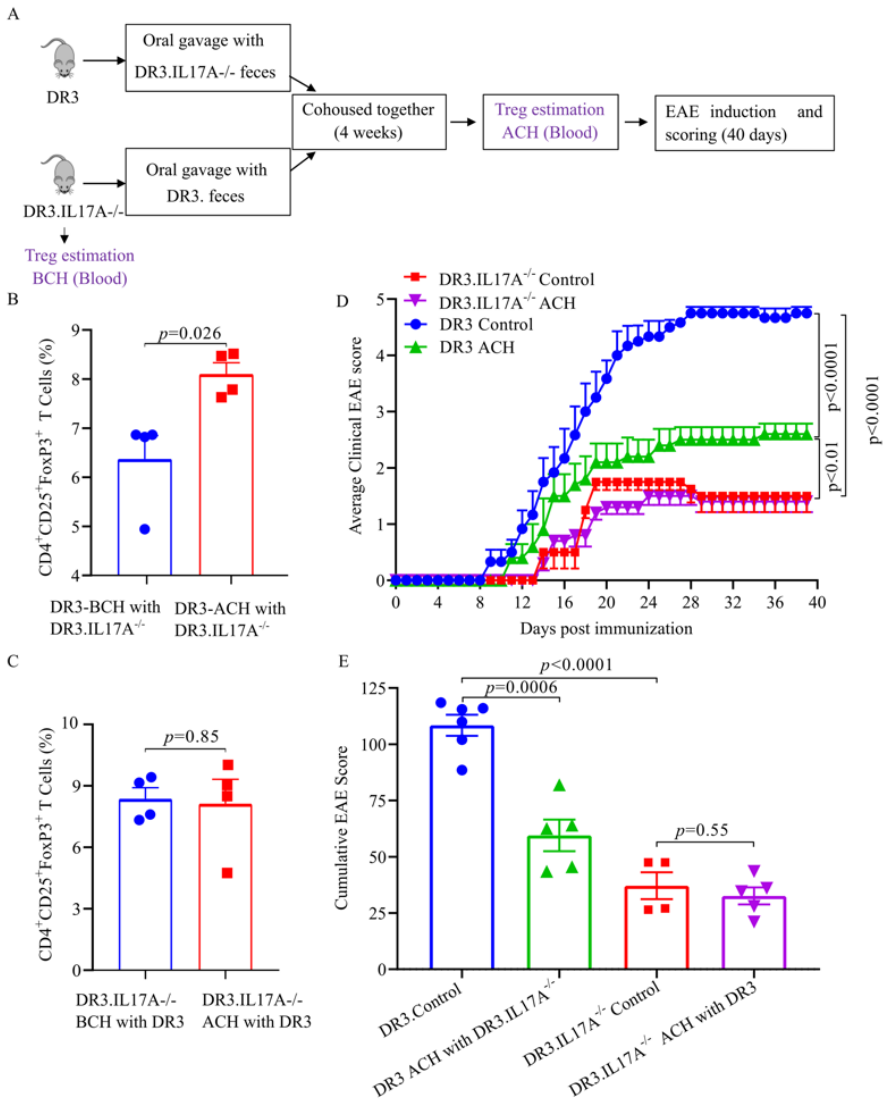

Fig. 5: Treg-inducing bacteria from DR3.IL17A$^{-/-}$ mice reduce disease severity when transferred to DR3 mice. (A) Schematic of experimental design showing experimental outline. 8-10-week-old female DR3 transgenic mice were cohoused for four weeks with DR3.IL17A$^{-/-}$ transgenic mice after one-time fecal transferred (orally gavaged) from each other mice strains. Peripheral blood mononuclear cells (PBMCs) were isolated from blood that was collected by retro-orbital bleeding, and regulatory T cells were assessed by flow cytometric analysis. Percentages of CD4^{+}CD25^{+}FoxP3^{+} T cell populations in (**B**) DR3 transgenic mice before (BCH) and after (ACH) being cohoused with DR3.IL17A$^{-/-}$ transgenic mice and in (**C**) DR3.IL17A$^{-/-}$ transgenic mice before (BCH) and after (ACH) being cohoused with DR3 transgenic mice. (**D**) Average clinical EAE scores of DR3 transgenic mice (non-cohoused control and after cohoused with DR3.IL17A$^{-/-}$ transgenic mice) and DR3.IL17A$^{-/-}$ transgenic mice (non-cohoused control and after cohoused

with DR3 transgenic mice) that were immunized with PLP_{91-110}/CFA and followed for 30 days. (**E**) Average cumulative EAE scores of mice in C. Data represent the mean and standard error of the mean for each experimental group from two independent experiments: n ≥4 mice per group. *p*-value was determined by unpaired t-test with Welch correction (A, B, D), two-way ANOVA for clinical EAE scores (C).

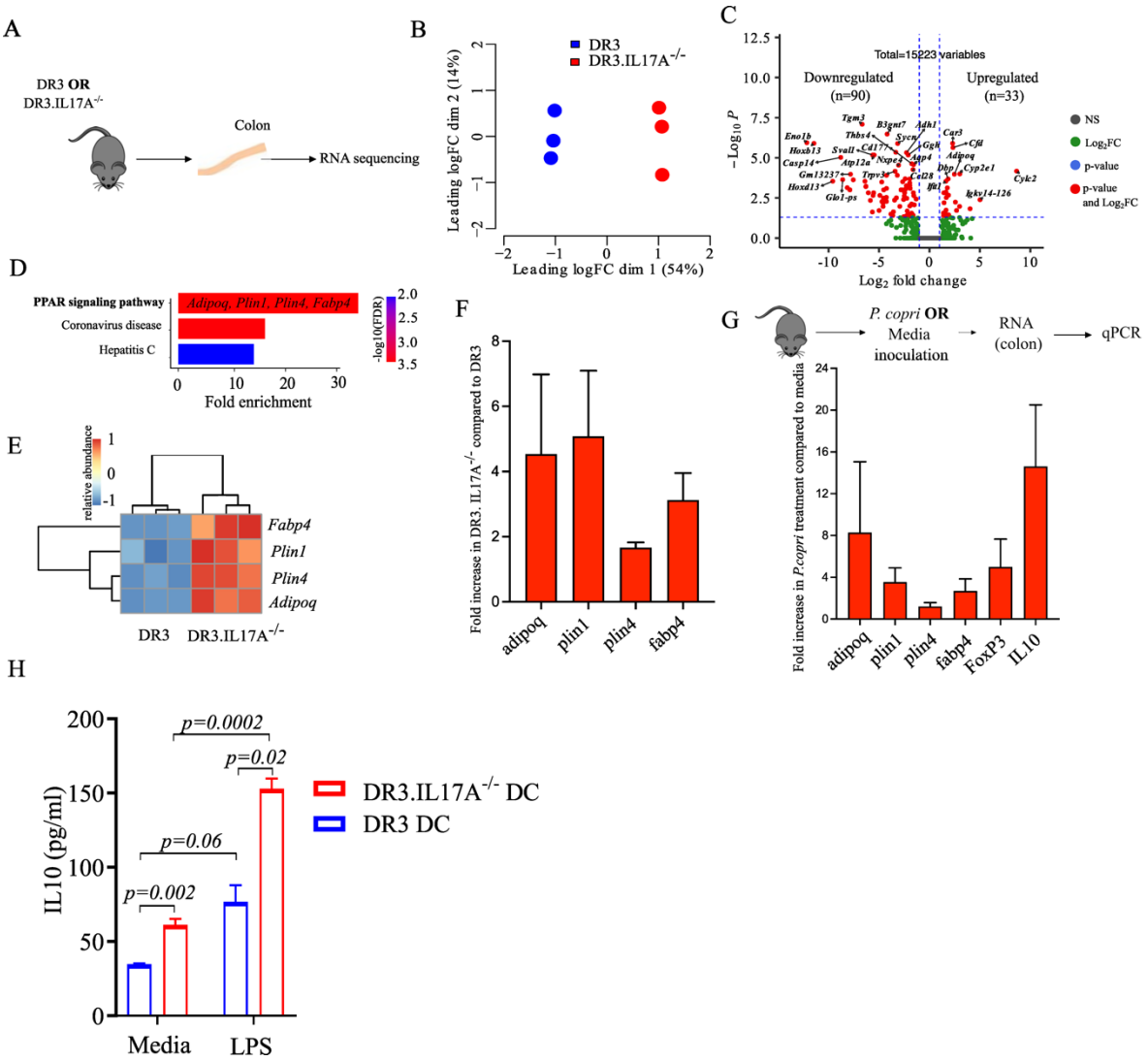

Fig. 6: DR3 and DR3.IL17A$^{-/-}$ transgenic mice exhibit distinct anti-inflammatory gene expression patterns in the colon. Colonic tissue was harvested from DR3 (n=3) or DR3.IL-17A$^{-/-}$ transgenic mice (n=3) and subjected to RNA-seq analysis**.** (**A**) Schematic diagram of workflow.

934 B) Multi-dimensional scaling plot showing the separation of DR3 and DR3.IL17A$^{-/-}$ colonic
935 samples. Each letter represents an RNA-Seq sample. Sample groups are indicated by different
936 colors, as indicated in the legend. (**C**) Volcano plot displaying the pattern of gene expression of
937 DR3.IL17A$^{-/-}$ mice relative to DR3 mice. Genes that are significantly differentially expressed, with
938 a Log_2 fold change of >1 and an FDR-corrected p-value <0.05, are highlighted in red, blue lines
939 represents the boundary for Log_2 fold change and the adjusted p-value cutoff. D) Pathways
940 enriched for 33 upregulated genes in KEGG database identified using ShinyGO webserver (37).
941 E) Heatmap of enriched genes in PPAR signaling pathway. F) Ratio of average fold change
942 expression of genes using qPCR related to PPAR signaling pathway in DR3.IL-17A$^{-/-}$ transgenic
943 mice to DR3 transgenic mice. G) Effect of *Prevotella copri* DSM 18205 supplementation in the colon
944 of DR3 mice**.** Mice (n = 5 in each group) were treated with either *P. copri* DSM 18205 (10^7 CFU) or media
945 (control) for every alternate day for two weeks. After two weeks, mice were euthanized, and RNA was
946 isolated from the colonic tissue. Genes related to PPAR pathways along with FoxP3 and IL-10 were
947 quantified using qPCR. Ratio of average fold change expression of genes related to PPAR signaling
948 pathway along with FOXP3 and IL10 in *P. copri* treated to media treated mice. (H) Quantification
949 of IL-10 cytokine production in naïve dendritic cells from DR3 and DR3.IL17A$^{-/-}$ transgenic mice
950 following stimulation with LPS. Splenocytes were harvested from naïve 8-10-week-old HLA-DR3
951 and DR3.IL17A$^{-/-}$ transgenic mice and CD11c+ dendritic cells were isolated using BD™ IMag
952 Particles. Purified CD11c+ cells were activated with LPS for 24 hours and IL-10 was measured
953 by ELISA. Media without LPS was used as control. Bars represent the mean and standard error of
954 the mean from each experimental group; n ≥3 mice per group. p-value was determined by pairwise
955 Mann-Whitney test.
956
957
958
959
960
961
962
963
964

965 **Supplementary Figures**

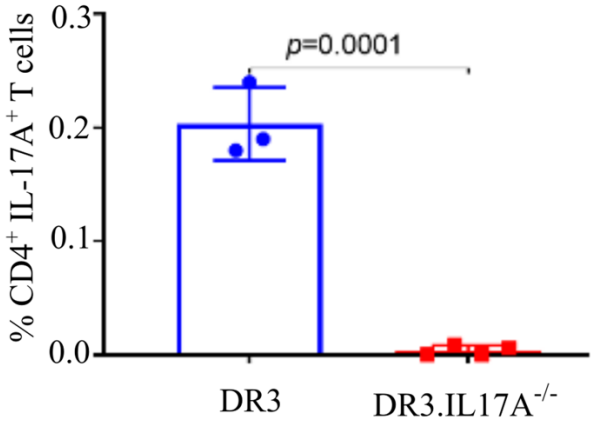

966

967 **Fig. S1: DR3.IL17A$^{-/-}$ mice lack IL-17A-expressing CD4+ T cells in the spleen.** 8-10-week-old
968 DR3 and DR3.IL17A$^{-/-}$ transgenic mice were euthanized and splenocytes were harvested for
969 analysis. Quantification of the frequency of CD4^{+}IL-17A^{+} T cells from mice in A. DR3: n=3;
970 DR3.IL17A$^{-/-}$: n = 4. *p*-value was determined using Mann-Whitney test between the experimental
971 groups. Symbols represent individual mice, bars represent mean±SEM.

972
973
974
975
976
977
978
979
980
981
982
983
984
985
986

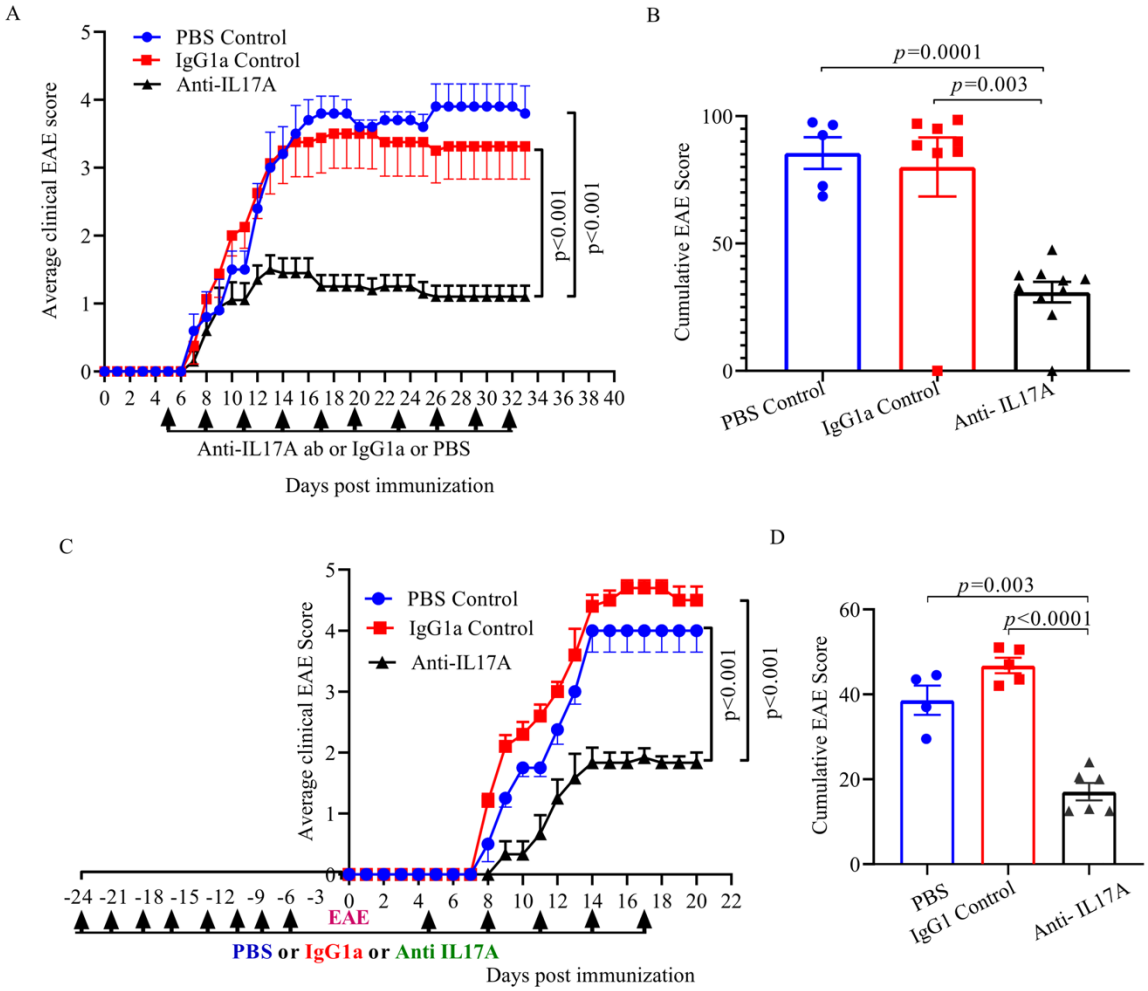

Fig. S2: Anti-IL-17A treatment lowers the severity of MOG_{35-55} induced EAE in C57BL/6J mice. (A-B) 8-10-week-old B6 mice were immunized with MOG_{35-55}/CFA. Five days after immunization, mice received anti-mouse IL-17A monoclonal antibody, isotype control mouse IgG1, or PBS intraperitoneally every three days until the end of the experiment (day 32). (A) Average clinical EAE scores over time. Treatment days are indicated by arrowheads. (B) Average cumulative EAE scores. (**C-D**) 8-10-week-old B6 mice were treated every three days with anti-IL-17A, IgG1, or PBS pre- and post-immunization with MOG_{35-55}/CFA. (C) Average clinical EAE scores. Treatment days are indicated by arrowheads. (D) Average cumulative EAE scores. For plots in A, C, each bullet point represents the mean and bars represent the standard error of the mean from each experimental group. *p*-value was determined using two-way ANOVA following Tukey correction for EAE clinical scores (A, C) and unpaired t-test with Welch correction for cumulative EAE score (B, D). For graphs in B, D, each bar represents mean±SEM.

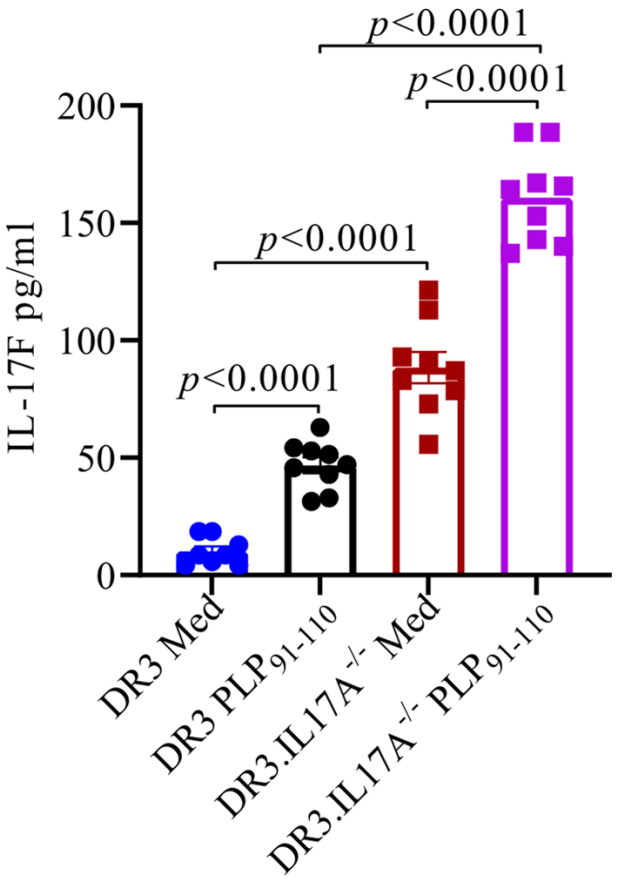

Fig. S3: Levels of inflammatory cytokines IL-17F in DR3 and DR3.IL17A$^{-/-}$ mice. 8-10-week-old mice were immunized with PLP_{91-110} /CFA to induce EAE. After 20 days, mice were euthanized, spleens were harvested, and splenic cells were cultured in the presence of PLP_{91-110} antigen for five days following stimulation with Phorbol myristate acetate (PMA) and ionomycin in the presence of Brefeldin A (BFA). The supernatant was collected and levels of IL17F were measured using ELISA. Cytokine values from DR3 mice were compared to those of DR3.IL17A$^{-/-}$ mice in either media (Med) or after stimulation with PLP_{91-110}. *p*-value was determined using unpaired t-test with Welch correction. Bars represent mean±S.E.M.

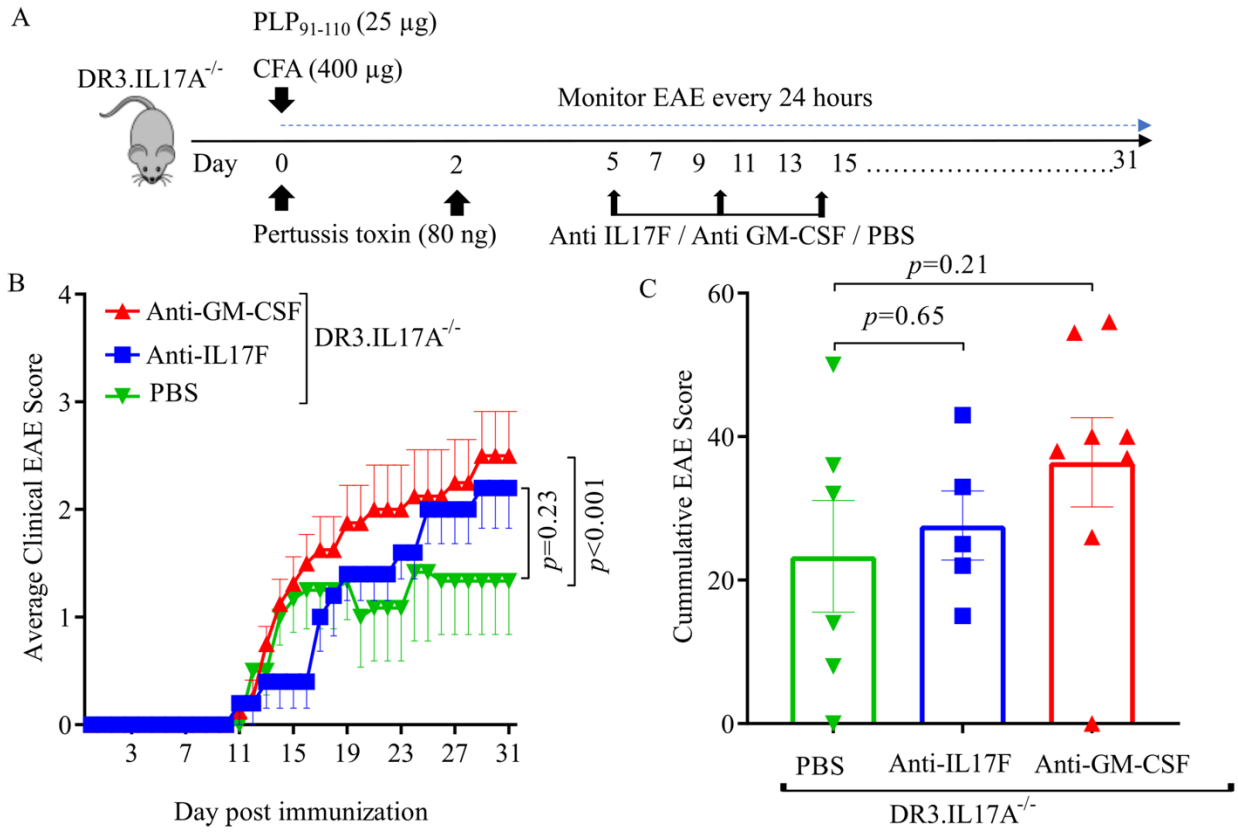

Fig. S4: Treatment with anti-GM-CSF or anti-IL-17F monoclonal antibodies increases disease severity in DR3.IL17A$^{-/-}$ mice. (**A**) Schematic diagram of the experimental workflow. EAE was induced in 8-10-week-old in DR3.IL17A$^{-/-}$ transgenic mice. At days 5, 10, and 14 post-EAE induction, mice received intraperitoneal injections of either: 1) anti-GM-CSF monoclonal antibody, 2) anti-IL-17F monoclonal antibody, or 3) IgGa1 isotype control and clinical EAE scores were monitored for 31 days. (**B**) Average clinical EAE score of mice in each group over time. Bullet points represent the mean and bars represent the standard error of the mean of each experimental group from two independent experiments (n ≥3 mice per group). *p*-value was determined by a two-way ANOVA following Tukey correction for average clinical EAE score (B). (**C**) Average cumulative EAE scores. *p*-value was determined by unpaired t-test with Welch correction (C). For plots in B, C, each symbol represents the mean and bars represent the standard error of the mean from each experimental group.

1032

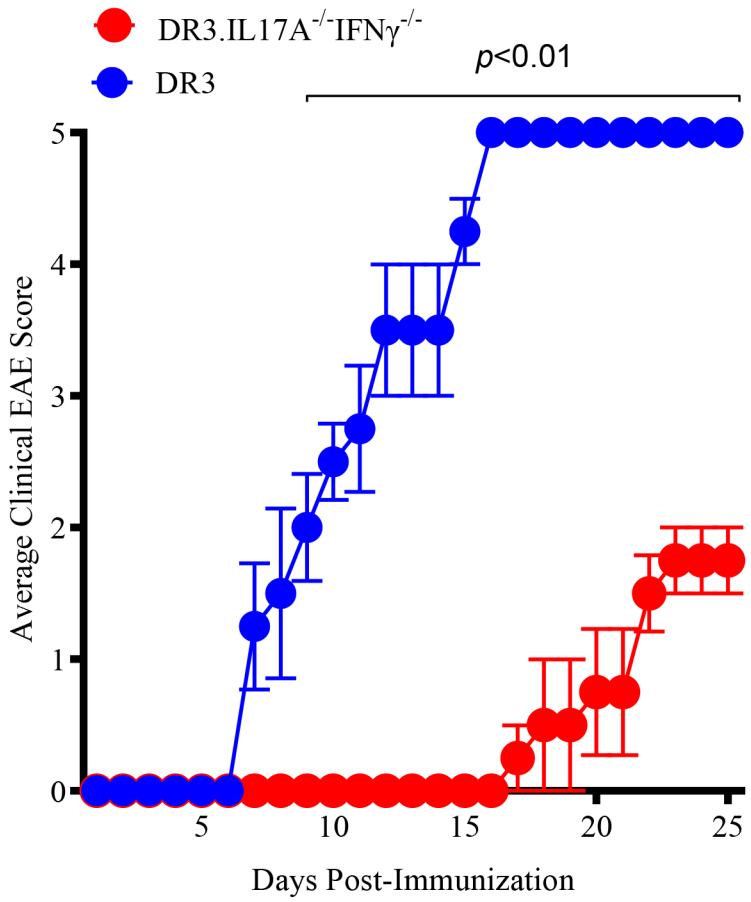

1033

1034 **Fig. S5: DR3.IL17A$^{-/-}$ mice develops milder EAE in absence of IFNγ .** EAE was induced in 8-
1035 10-week-old in DR3 and DR3.IL17A$^{-/-}$IFNγ$^{-/-}$ transgenic mice using PLP$_{91-110}$, CFA and PTX.
1036 The disease was monitored and scored daily until day 25 of the experiment. Average clinical
1037 EAE score of mice in each group over time. Bullet points represent the mean and bars represent
1038 the standard error of the mean of each experimental group from two independent experiments (n
1039 =4 mice per group). *p*-value was determined by multiple unpaired t-tests with correction using
1040 two-stage step up method of Benjamini, Krieger and Yekutieli for average clinical EAE score.

1041

1042

1043

1044

1045

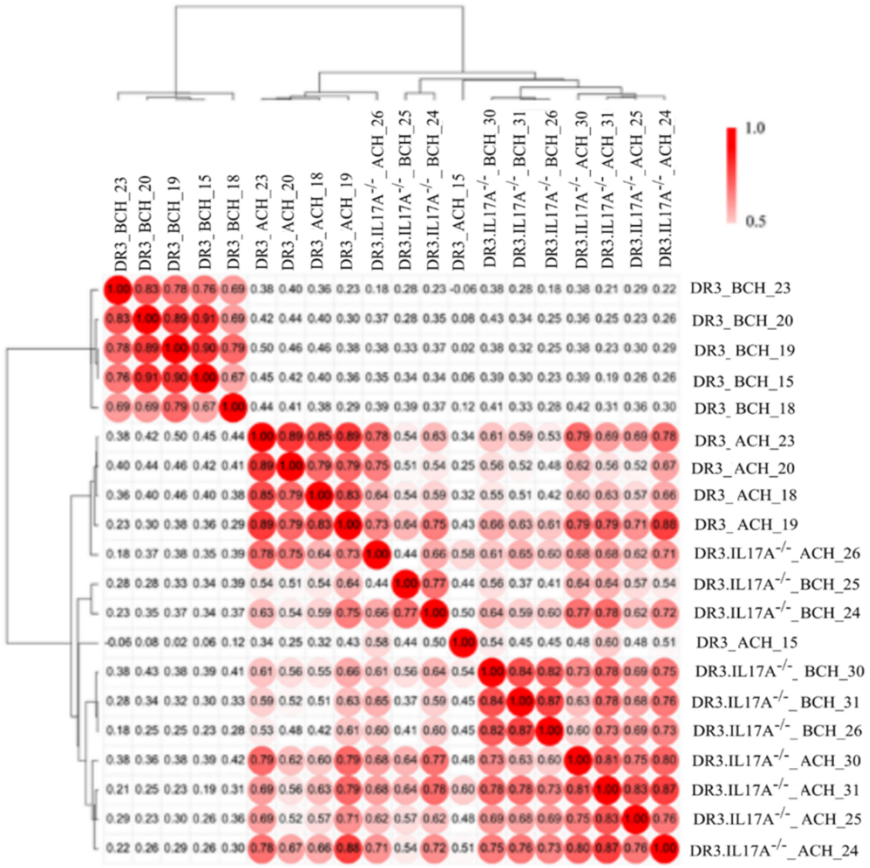

Fig. S6: Similarity matrix of microbial compositional communities present in DR3 and DR3.IL17A$^{-/-}$ mice before (BCH) and after (ACH) cohousing. Matrix was computed from the relative abundance matrix using 1-Spearman rank correlation metric using average linkage method and clustered hierarchically using Morpheus webserver (https://software.broadinstitute.org/morpheus).

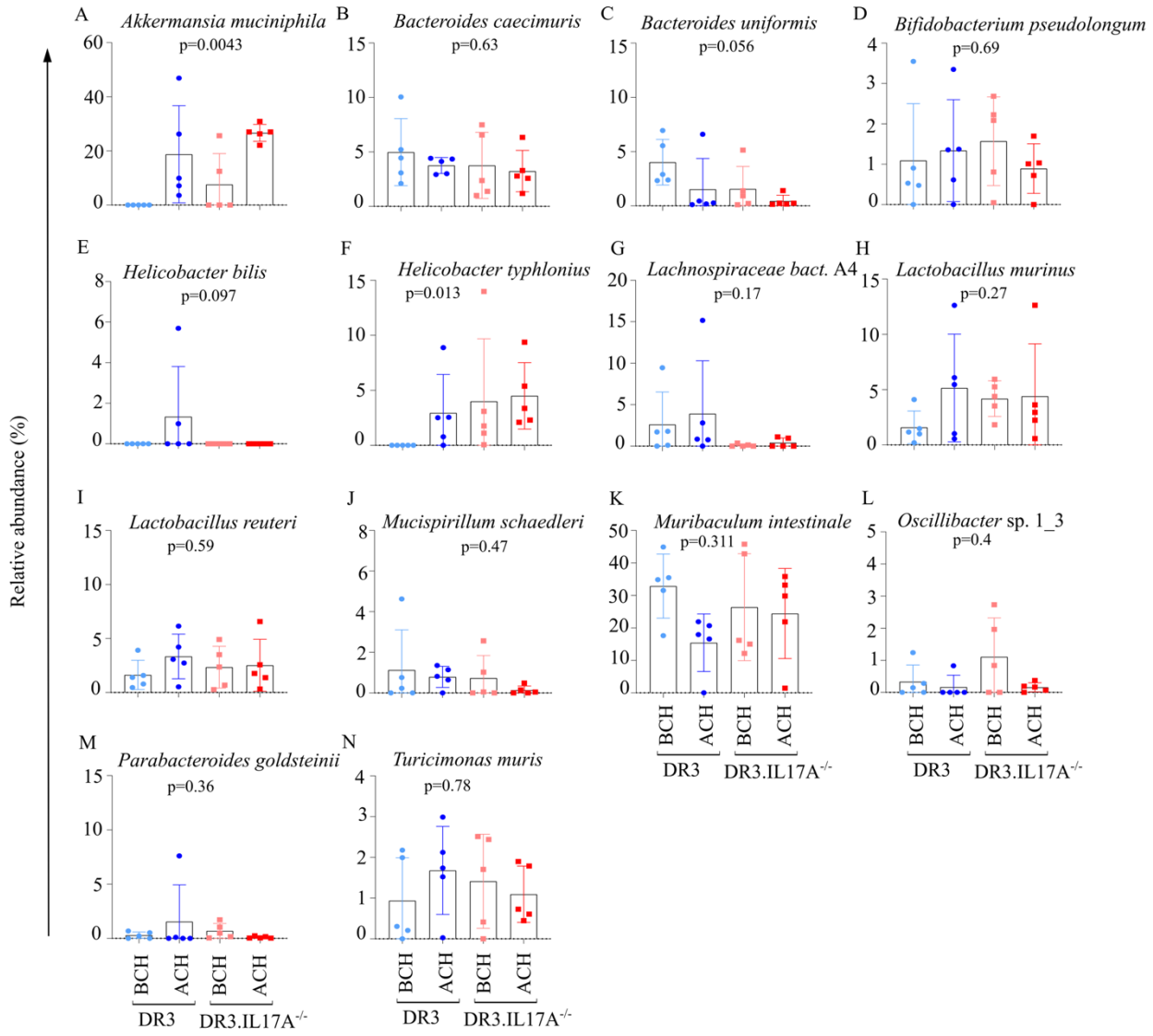

Fig. S7: Composition of the gut bacteria in DR3 and DR3.IL17A$^{-/-}$ transgenic mice before (BCH) and after (ACH) mice were cohoused. Each bar represents the average relative abundance (%) of the bacterium in each group. Kruskal Wallis test followed by Dunn-test was performed to identify the significance between the groups. 'p-value' from A-N represents the significance for the Kruskal Wallis test. Those bacteria with significant/non-significant p-value from Kruskal Wallis test but non-significantly different in at least one of the groups of interest (DR3-BCH to DR3.IL17A$^{-/-}$-BCH, DR3-BCH to DR3-ACH and DR3.IL17A$^{-/-}$-BCH to DR3.IL17A$^{-/-}$-ACH) following Dunn test are shown.

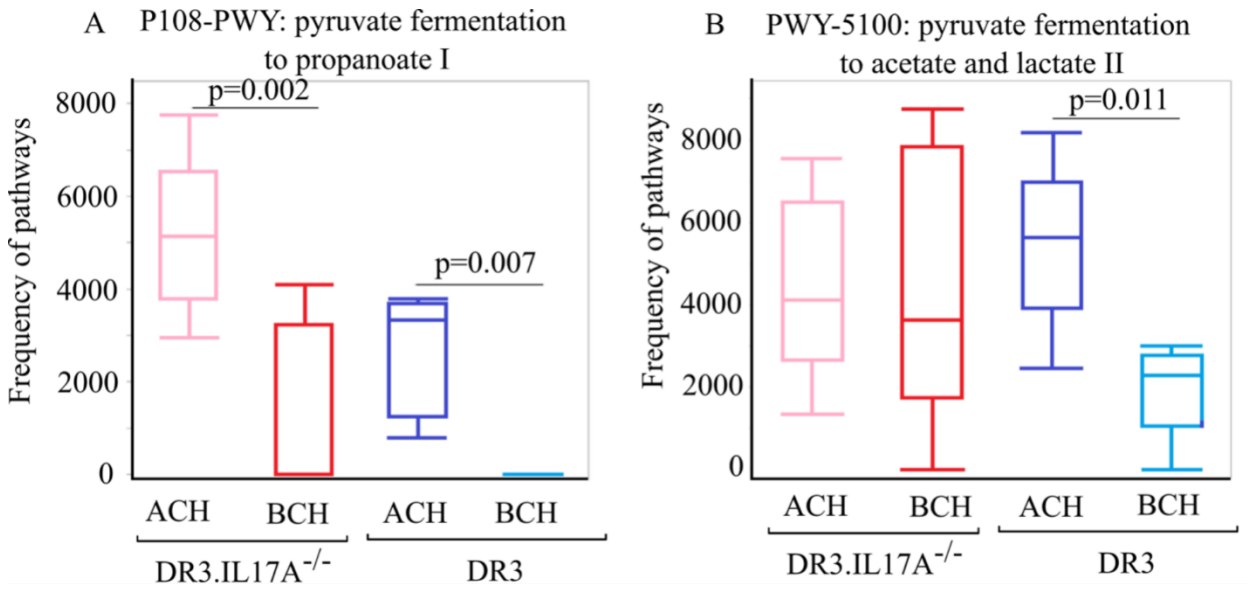

Fig. S8: Abundance of short chain fatty acid pathways, as determined by shotgun metagenomics analysis in DR3.IL17A$^{-/-}$ and DR3 transgenic mice before (BCH) and after (ACH) they were cohoused. Pairwise Wilcoxon test was performed to obtain the statistical significance BCH and ACH for each DR3 and DR3.IL17A$^{-/-}$ transgenic mice.

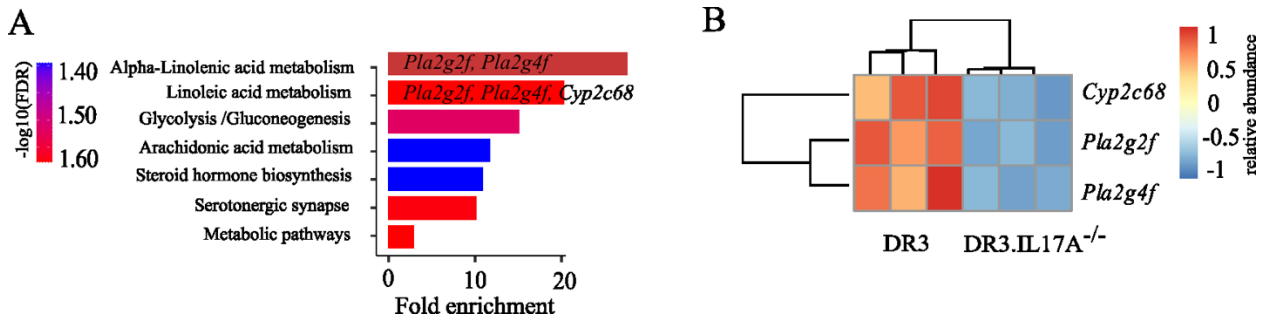

Fig. S9: **DR3 and DR3.IL17A$^{-/-}$ transgenic mice exhibit distinct gene expression patterns in the colon.** Colonic tissue was harvested from DR3 (n=3) or DR3.IL-17A$^{-/-}$ transgenic mice (n=3) and subjected to RNA-seq analysis. A) Pathways enriched for 90 downregulated genes in KEGG database identified using ShinyGO webserver (37). B) Heatmap of enriched genes in alpha-linolenic and linoleic acid metabolism pathway. F) Expression of genes related to alpha-linolenic and linoleic acid metabolism pathway in DR3 or DR3.IL-17A$^{-/-}$ transgenic mice.

1105 **Tables:**

1106 **Table S1:** Differentially expressed gene list in the colon of DR3.IL17A$^{-/-}$ compared to DR3
1107 transgenic mice calculated using *limma* package within *edgeR* in R. All 123 differentially
1108 expressed genes with *LogFC*>1.0 and *adj.p.val*<0.05 are shown.

SN	Genes	logFC	AveExpr	t	P.Value	adj.P.Val
1	Eno1b	-12.154	1.443	-19.576	0.000	0.000
2	Hoxb13	-11.448	-1.890	-19.897	0.000	0.000
3	Hoxd13	-9.589	-1.902	-10.871	0.000	0.000
4	Casp14	-8.793	-1.658	-13.128	0.000	0.000
5	Glo1-ps	-8.601	-0.491	-9.588	0.000	0.000
6	2310079G19Rik	-8.148	-2.842	-8.433	0.000	0.000
7	Rpl15-ps6	-7.886	0.116	-6.560	0.000	0.002
8	Gm13237	-7.823	-0.170	-8.445	0.000	0.000
9	Ly6g	-7.548	-2.237	-11.113	0.000	0.000
10	Tgm3	-6.671	3.560	-31.635	0.000	0.000
11	Vtcn1	-6.393	-3.095	-8.575	0.000	0.000
12	Mettl7a2	-6.307	-3.303	-8.664	0.000	0.000
13	Igkv8-18	-6.293	-0.666	-8.186	0.000	0.000
14	Fxyd4	-6.059	-1.910	-4.809	0.000	0.025
15	5033404E19Rik	-5.855	-2.774	-5.566	0.000	0.008
16	Gm7334	-5.659	1.342	-5.672	0.000	0.007
17	Sval1	-5.631	3.704	-19.493	0.000	0.000
18	Evx2	-5.587	-2.795	-6.518	0.000	0.002
19	Gm8540	-5.532	-3.496	-7.667	0.000	0.000
20	Atp12a	-5.477	0.033	-18.752	0.000	0.000
21	Chit1	-4.989	-3.144	-5.998	0.000	0.004
22	Trpv6	-4.912	-0.557	-8.873	0.000	0.000
23	Igkv2-112	-4.725	1.275	-9.585	0.000	0.000
24	Fut9	-4.701	-1.951	-6.631	0.000	0.002

25	Ighv7-1	-4.595	0.648	-6.919	0.000	0.001
26	Ninj2	-4.593	-1.906	-5.754	0.000	0.006
27	St8sia5	-4.551	-1.819	-5.220	0.000	0.013
28	Ighv1-61	-4.532	1.365	-7.272	0.000	0.001
29	Tmprss13	-4.269	-0.183	-8.813	0.000	0.000
30	Gjb5	-4.261	-1.541	-4.778	0.000	0.025
31	Hoxd12	-4.259	-3.247	-4.345	0.000	0.049
32	Vsig1	-4.255	-1.212	-6.516	0.000	0.002
33	Ighv10-3	-4.253	3.640	-11.518	0.000	0.000
34	B3gnt7	-4.195	5.973	-34.648	0.000	0.000
35	Rpl15-ps2	-3.829	-0.635	-4.963	0.000	0.019
36	Itih2	-3.817	-1.521	-4.471	0.000	0.041
37	Mettl7a3	-3.571	-1.774	-4.445	0.000	0.042
38	Pla2g4f	-3.458	0.531	-5.797	0.000	0.006
39	Trpv3	-3.403	3.252	-12.943	0.000	0.000
40	Thbs4	-3.334	3.057	-21.508	0.000	0.000
41	Hoxa13	-3.280	-1.700	-8.765	0.000	0.000
42	Itln1	-3.187	6.879	-10.731	0.000	0.000
43	Sycn	-3.151	2.937	-24.593	0.000	0.000
44	Nxpe4	-3.057	3.610	-15.040	0.000	0.000
45	Insl5	-2.941	-1.314	-6.488	0.000	0.002
46	Ighv2-5	-2.897	2.075	-4.897	0.000	0.021
47	Adgrf1	-2.818	0.607	-9.433	0.000	0.000
48	Igkv3-4	-2.711	3.280	-8.454	0.000	0.000
49	Igkv4-57	-2.655	4.588	-12.494	0.000	0.000
50	Slc28a3	-2.572	2.546	-4.625	0.000	0.032
51	Igkv4-68	-2.565	4.316	-8.356	0.000	0.000
52	Pla2g2f	-2.494	3.879	-7.097	0.000	0.001

53	Ighv3-3	-2.458	1.456	-8.997	0.000	0.000
54	Cyp2d12	-2.407	1.294	-9.324	0.000	0.000
55	Best2	-2.363	0.866	-10.732	0.000	0.000
56	Gm47283	-2.290	5.085	-10.117	0.000	0.000
57	Adh1	-2.274	5.559	-21.681	0.000	0.000
58	Ighv1-39	-2.271	3.886	-4.873	0.000	0.022
59	Cyp2c68	-2.248	4.529	-8.006	0.000	0.000
60	B3gnt5	-2.203	3.517	-6.569	0.000	0.002
61	Ighv5-4	-2.151	2.640	-5.001	0.000	0.018
62	Ggh	-2.100	5.137	-16.144	0.000	0.000
63	Cyp2d9	-2.078	0.066	-4.490	0.000	0.040
64	Zfp791	-2.041	2.587	-4.591	0.000	0.034
65	Slc15a2	-2.026	2.158	-4.924	0.000	0.020
66	Nox1	-2.008	3.528	-7.361	0.000	0.001
67	Nt5e	-1.973	5.284	-10.629	0.000	0.000
68	Duoxa2	-1.952	6.303	-10.058	0.000	0.000
69	Ang4	-1.951	7.834	-9.720	0.000	0.000
70	Ighv2-9-1	-1.949	3.374	-4.962	0.000	0.019
71	Slc15a1	-1.948	6.682	-8.009	0.000	0.000
72	Igkv3-5	-1.942	3.424	-5.541	0.000	0.008
73	Cldn8	-1.909	4.312	-9.203	0.000	0.000
74	Eno3	-1.762	3.750	-6.374	0.000	0.002
75	Clic6	-1.762	3.833	-5.762	0.000	0.006
76	Cd177	-1.749	6.807	-16.983	0.000	0.000
77	Adamts15	-1.691	4.728	-5.747	0.000	0.006
78	Ccl28	-1.628	7.068	-12.416	0.000	0.000
79	Igkv9-120	-1.622	4.390	-4.733	0.000	0.027
80	Hoxa11	-1.621	0.018	-5.452	0.000	0.009

81	Ceacam10	-1.593	5.986	-8.932	0.000	0.000
82	Aqp4	-1.573	6.556	-14.118	0.000	0.000
83	Saa1	-1.550	7.353	-7.683	0.000	0.000
84	Ano1	-1.550	3.699	-6.163	0.000	0.003
85	Tcf7l1	-1.529	2.331	-4.795	0.000	0.025
86	Cela1	-1.499	4.613	-7.343	0.000	0.001
87	Gm15401	-1.437	3.493	-4.550	0.000	0.036
88	Prdx6	-1.317	8.165	-8.030	0.000	0.000
89	Retnlb	-1.259	5.150	-4.445	0.000	0.042
90	Scd2	-1.133	9.600	-5.131	0.000	0.015
91	Plin4	1.287	6.266	4.615	0.000	0.033
92	Cyp4b1	1.379	4.923	4.760	0.000	0.026
93	Slc13a1	1.393	7.159	5.688	0.000	0.006
94	Hbb-bs	1.412	5.567	5.082	0.000	0.016
95	Naaladl1	1.451	8.878	5.901	0.000	0.005
96	Oas2	1.473	3.640	4.420	0.000	0.044
97	Tef	1.533	4.008	5.337	0.000	0.011
98	Oasl2	1.568	5.620	8.209	0.000	0.000
99	Fabp4	1.636	8.267	8.666	0.000	0.000
100	Ifit1	1.636	6.835	13.024	0.000	0.000
101	Rpl3	1.638	7.213	9.483	0.000	0.000
102	Thrsp	1.641	5.122	4.949	0.000	0.020
103	Ddx60	1.649	4.067	6.229	0.000	0.003
104	Ifit3	1.670	4.893	6.902	0.000	0.001
105	Retn	1.716	4.432	5.022	0.000	0.018
106	Sis	1.727	7.589	5.489	0.000	0.009
107	Igkv12-98	1.757	2.715	4.414	0.000	0.044
108	Oas3	1.774	4.742	8.831	0.000	0.000

109	Dbp	1.855	4.802	9.977	0.000	0.000
110	Rpl15	1.893	7.014	8.315	0.000	0.000
111	Igkv14-100	1.910	3.744	5.128	0.000	0.015
112	Car3	2.300	7.529	24.744	0.000	0.000
113	Cfd	2.334	7.125	24.230	0.000	0.000
114	Adipoq	2.474	4.756	11.111	0.000	0.000
115	Plin1	2.574	4.541	7.430	0.000	0.001
116	Lgals2	2.688	5.834	6.063	0.000	0.004
117	Tcaim	2.984	2.326	6.378	0.000	0.002
118	Trgc2	2.984	1.211	4.446	0.000	0.042
119	Cyp2e1	3.009	5.145	15.014	0.000	0.000
120	Lyrm7	3.114	0.716	4.632	0.000	0.032
121	Gm16011	4.232	-0.321	4.370	0.000	0.047
122	Igkv14-126	5.013	0.842	7.976	0.000	0.000
123	Cylc2	8.644	-1.325	9.999	0.000	0.000

1109